4-1-2013

# The Low-Resolution Structure of Nascent High Density Lipoprotein Reconstituted with DMPC With and Without Cholesterol Reveals A Mechanism for Particle Expansion

Valentin Gogonea
*Cleveland State University*, V.GOGONEA@csuohio.edu

Gary S. Gerstenecker
*Cleveland State University*

Zhiping Wu
*Cleveland Clinic*

Xavier Lee
*Cleveland Clinic*

Celalettin Topbas
*Cleveland State University*

# The low-resolution structure of nHDL reconstituted with DMPC with and without cholesterol reveals a mechanism for particle expansion[S]

**Valentin Gogonea,[1,*,†,§] Gary S. Gerstenecker,[*,§] Zhiping Wu,[*,†] Xavier Lee,[*,†] Celalettin Topbas,[*,§] Matthew A. Wagner,[*,†] Thomas C. Tallant,[*,†] Jonathan D. Smith,[*] Philip Callow,[**] Vitaliy Pipich,[††] Hélène Malet,[§§] Guy Schoehn,[§§,***] Joseph A. DiDonato,[*,†] and Stanley L. Hazen[1,*,†,†††]**

Department of Cellular and Molecular Medicine,* Center for Cardiovascular Diagnostics and Prevention,† and Department of Cardiovascular Medicine,††† Cleveland Clinic, Cleveland, OH; Department of Chemistry,§ Cleveland State University, Cleveland, OH; Institut Laue-Langevin,** BP 156, 38042 Grenoble Cedex 9, France; Jülich Center for Neutron Science at FRM II,†† 85747 Garching, Germany; Unit for Virus Host Cell Interactions,§§ UMI 3265 (CNRS-EMBL-UJF), BP 181, F38042 Grenoble France; CEA, CNRS, and Université Joseph Fourier,*** Institut de Biologie Structurale Jean-Pierre Ebel, UMR5075 Grenoble, France

**Abstract Small-angle neutron scattering (SANS) with contrast variation was used to obtain the low-resolution structure of nascent HDL (nHDL) reconstituted with dimyristoyl phosphatidylcholine (DMPC) in the absence and presence of cholesterol, [apoA1:DMPC (1:80, mol:mol) and apoA1:DMPC:cholesterol (1:86:9, mol:mol:mol)]. The overall shape of both particles is discoidal with the low-resolution structure of apoA1 visualized as an open, contorted, and out of plane conformation with three arms in nascent HDL/dimyristoyl phosphatidylcholine without cholesterol ($nHDL_{DMPC}$) and two arms in nascent HDL/dimyristoyl phosphatidylcholine with cholesterol ($nHDL_{DMPC+Chol}$). The low-resolution shape of the lipid phase in both $nHDL_{DMPC}$ and $nHDL_{DMPC+Chol}$ were oblate ellipsoids, and fit well within their respective protein shapes. Modeling studies indicate that apoA1 is folded onto itself in $nHDL_{DMPC}$, making a large hairpin, which was also confirmed independently by both cross-linking mass spectrometry and hydrogen-deuterium exchange (HDX) mass spectrometry analyses. In $nHDL_{DMPC+Chol}$, the lipid was expanded and no hairpin was visible. Importantly, despite the overall discoidal shape of the whole particle in both $nHDL_{DMPC}$ and $nHDL_{DMPC+Chol}$, an open conformation (i.e., not a closed belt) of apoA1 is observed. Collectively, these data show that full length apoA1 retains an open architecture that is dictated by its lipid cargo. The lipid is likely predominantly organized as a bilayer with a micelle domain between the open apoA1 arms. The apoA1 configuration observed suggests a mechanism for accommodating changing lipid cargo by quantized expansion of hairpin structures.—**Gogonea, V., G. S. Gerstenecker, Z. Wu, X. Lee, C. Topbas, M. A. Wagner, T. C. Tallant, J. D. Smith, P. Callow, V. Pipich, H. Malet, G. Schoehn, J. A. DiDonato, and S. L. Hazen. **The low-resolution structure of nHDL reconstituted with DMPC with and without cholesterol reveals a mechanism for particle expansion. *J. Lipid Res.* 2013.** 54: **966–983.**

**Supplementary key words** nascent high density lipoprotein • apolipoprotein A1 • dimyristoyl phosphatidylcholine • small-angle neutron scattering

Cholesterol from peripheral tissues, such as within the artery wall, is transported to the liver by high density lipoprotein (HDL) particles, which are continuously remodeled in a process called reverse cholesterol transport (1, 2). HDL particles are highly heterogeneous, varying in protein and lipid content (3). Apolipoprotein A1 (apoA1) is

*This study was supported by National Institutes of Health Grants P01 HL-098055, P01 HL-076491, and by the Leduc Foundation. S.L.H. was partially supported by a gift from the Leonard Krieger Fund and V.G. acknowledges the Faculty Development Research Award from Cleveland State University. The electron microscopy facility used is part of the Grenoble Partnership for Structural Biology. Computational resources were provided by the Ohio Supercomputer Center and the National Center for Supercomputer Applications (NCSA, University of Illinois). Mass Spectrometry instrumentation used was housed within the Cleveland Clinic Mass Spectrometry Facility with partial support through a Center of Innovation by AB SCIEX. Some of the human apoA1 used in this study was purified from HDL provided as a generous gift from CSL Limited (Victoria, Australia).*

*Manuscript received 28 September 2012 and in revised form 17 January 2013.*

*Published, JLR Papers in Press, January 23, 2013*
*DOI 10.1194/jlr.M032763*

Abbreviations: DMPC, dimyristoyl phosphatidylcholine; DSH, double super helix; ESR, electron spin resonance; FRET, fluorescence resonance energy transfer; HDX, hydrogen-deuterium exchange; LUV, large unilamellar vesicle; nHDL, nascent HDL; $nHDL_{DMPC}$, nascent HDL/dimyristoyl phosphatidylcholine without cholesterol; $nHDL_{DMPC+Chol}$, nascent HDL/dimyristoyl phosphatidylcholine with cholesterol; $nHDL_{POPC}$, nascent HDL/POPC and cholesterol; PC, phosphatidyl choline; POPC, 1-palmitoyl-2-oleoyl-*sn*-glycero-3-phosphocholine; *q*, range of momentum transfer; SANS, small-angle neutron scattering; SCX, strong-cation exchange.

[1] To whom correspondence should be addressed.
e-mail: v.gogonea@csuohio.edu (V.G.); e-mail: hazens@ccf.org (S.L.H.)

[S] The online version of this article (available at http://www.jlr.org) contains supplementary data in the form of 12 figures.

the major protein component of HDL, and plasma levels of both HDL cholesterol and apoA1 are inversely correlated with the incidence of cardiovascular diseases (3–5). A major focus of many ongoing pharmacologic interventions is HDL-targeted therapies, including direct infusion of reconstituted and fully biologically functional nascent HDL (nHDL) particles (4). Despite its importance to many biological and biomedical functions, the high-resolution structures of various HDL particles are yet to be resolved.

Nevertheless, various models of nHDL have been proposed in the past (6, 7), and they rely on biophysical, biochemical, and computer simulation studies [e.g., the Picket Fence model (8), the Belt model (9, 10), the Hairpin Loop models (11–13), the Solar Flares model (14), the Double Super Helix model (15), and the Twisted Belt model (16, 17)]. All current models have in common an antiparallel orientation of the two apoA1 chains, but the overall conformation of apoA1 within the particle is still a matter of intense debate (18). The amphipathic apoA1 chains in all models wrap around a central lipid core, and the orientation of amino acid residues along the apoA1 chains position the hydrophobic side chains toward the lipid surface. Before studies employing contrast variation small-angle neutron scattering (SANS) (see below), the overall conformation of apoA1 within a lipid containing HDL particles was inferred from crystal structure data from lipid free apoA1 mutant forms (19, 20), as well as measured distance constraints between inter- and intrachain amino acids in mutated or derivatized apoA1 using FRET or ESR (12), and in native apoA1 by cross-linking MS studies (11, 15, 21, 22). Further structural information has been obtained from amide bond hydrogen/deuterium exchange mass spectrometry (14, 23, 24)}, and cryo-electron tomography (25).

The recent application of contrast variation SANS to the structural interrogation of nHDL and spherical HDL particles has allowed for the first time direct visualization of the low-resolution shape envelope of the protein versus the lipid components of HDL (15, 26, 27). The structures revealed allowed for the possibility of developing models that incorporated the SANS shape constraints, giving a better understanding of how apoA1 and lipids within different forms of HDL are structurally organized. Among all nHDL models, only the Double Super Helix model (15) incorporated direct SANS imaging data of the low-resolution structures of apoA1 and the lipid domain of a recombinant biologically functional nHDL preparation reconstituted with 1-palmitoyl-2-oleoyl-*sn*-glycero-3-phosphocholine (POPC) (15). In contrast to longer chain PC molecular species, addition of apoA1 to dimyristoyl phosphatidylcholine (DMPC) vesicles spontaneously assembles HDL-like structures [presumed "discs" (28, 29)], and thus has been a focus of structural studies. While our initial SANS studies of nHDL focused on use of full length apoA1 and the longer chain and more physiologically relevant molecular species of PC (POPC), because of the dramatic differences in overall particle organization observed with the double super helix (DSH) model versus the earlier discoidal models based on computer simulations, we felt it reasonable to directly interrogate the structure of "DMPC discs" in nascent HDL/dimyristoyl phosphatidylcholine without cholesterol ($nHDL_{DMPC}$).

In a contrast variation SANS experiment the concentration of $D_2O$ in buffer is varied such that the scattering length density of the buffer matches that of a component within the particle (i.e., protein, lipid, or nucleic acid), making that component "transparent". In addition, by selectively deuterating specific components of a macromolecular assembly (in our case, apoA1, by producing the recombinant protein in *Escherichia coli* grown in $D_2O$ with deuterated nutrients), one can further enhance the contrast between different components within the complex and reduce the interference of the other component (the lipid in this case). The contrast variation experiment thus enables one to "triangulate" different components of a macromolecular complex, making SANS a powerful and unique structural interrogation tool (26, 30–32).

Herein we employ contrast variation SANS to directly visualize the individual low-resolution protein and lipid conformations within nHDL reconstituted using apoA1:DMPC (1:80) ($nHDL_{DMPC}$), as initially employed for the discoidal HDL model (29), and apoA1:DMPC:cholesterol (1:80:10) [nascent HDL/dimyristoyl phosphatidylcholine with cholesterol ($nHDL_{DMPC+Chol}$)]. Our studies reveal, remarkably, that despite overall "discoidal" particle shapes, apoA1 in both particles is not organized in a circumferential belt conformation, but instead, is open and slightly out of plane. In $nHDL_{DMPC}$ three arms of apoA1 enshrine a central oblate lipid core. One of the arms is a large hairpin, a configuration confirmed by cross-linking mass spectrometry, and further corroborated by H/D kinetic exchange analyses consistent with a large hairpin. On the other hand, in $nHDL_{DMPC+Chol}$ where the lipid core is 20% expanded, apoA1 is closer in conformation to a traditional double belt conformation, enshrining a less symmetric lipid phase, but nonetheless with open apoA1 conformation. The open apoA1 conformation observed coupled with the dimensions observed for the lipid core of both particles reveals a mechanism accounting for quantized particle size expansion frequently observed during nHDL formation, as well as suggests a lipid organization within the particle that possesses a combination of both lamellar (bilayer) and micellar configuration.

## MATERIALS AND METHODS

### Preparation of $nHDL_{DMPC}$ with and without cholesterol

The particle composition selected for our studies and the methods for particle generation and characterization are the same as those previously published (16, 33). Human apoA1 was isolated from HDL provided by CSL Limited (Victoria, Australia), as well as from plasma obtained from healthy volunteers who gave written informed consent under a protocol approved by the Cleveland Clinic Institutional Review Board. ApoA1 was purified from HDL isolated by ultracentrifugation (density range of 1.07–1.21 g/ml). Lipid-free human apoA1 was recovered by delipidation





JOURNAL OF LIPID RESEARCH ASBMB

of the HDL followed by ion exchange chromatography, as previously described (28). Recombinant human apoA1 was generated in *E. coli* and isolated as described in Ref. 34. The His tag of isolated recombinant apoA1 forms was removed by formic acid cleavage, and subsequent cleanup was done by nickel affinity chromatography and a polishing ion exchange chromatography step (14, 34). To obtain deuterated recombinant human apoA1, the kanamycin-resistant plasmid pET20b+ encoding 6× His-tagged human apoA1 was transformed into *E. coli* BL21(DE3) cells. Cells were grown in 85% deuterated minimal medium (85% $D_2O$, 15% $H_2O$): 6.86 g/l $(NH_4)_2SO_4$, 1.56 g/l $KH_2PO_4$, 6.48 g/l $Na_2HPO_4{\cdot}2H_2O$, 0.49 g/l diammonium hydrogen citrate, 0.25 g/l $MgSO_4{\cdot}7H_2O$, 1.0 ml $l^{-1}$ (0.5 g/l $CaCl_2{\cdot}2H_2O$, 16.7 g/l $FeCl_3{\cdot}6H_2O$, 0.18 g/l $ZnSO_4{\cdot}7H_2O$, 0.16 g/l $CuSO_4{\cdot}5H_2O$, 0.15 g/l $MnSO_4{\cdot}4H_2O$, 0.18 g/l $CoCl_2{\cdot}6H_2O$, 20.1 g/l EDTA), 40 mg/l kanamycin with hydrogenated glycerol as carbon source (5 g/l). Deuterated apoA1 was purified by nickel affinity chromatography as above and a polishing ion exchange chromatography step (14, 34). SDS-PAGE was used to assess the purity of isolated human and recombinant apoA1.

Because initial efforts to prepare nHDL preparations by DMPC-driven spontaneous particle formation led to inhomogeneous preparations, reconstituted $nHDL_{DMPC}$ with and without cholesterol was prepared using a modified sodium cholate dialysis method (35) at an initial molar ratio of 80:1 of DMPC:apoA1 or 10:80:1 of cholesterol:DMPC:apoA1. Subsequently, the HDL particles were purified by gel filtration chromatography using Sephacryl S300 (GE Healthcare) column. The size of reconstituted nHDL preparations were measured by using dynamic light scattering, and nondenaturing PAGE (14). The stoichiometry of each of the nHDL preparations was determined by quantifying apoA1 phospholipid content using the microphosphorous assay, and cholesterol content using stable isotope dilution mass spectrometry (14). The remaining sodium cholate in reconstituted nHDL preparations was also quantified by HPLC tandem mass spectrometry, which confirmed that no significant residual cholate was present (i.e., cholate content << 0.1 mol%). BS3 was used as a chemical cross-linker at a molar ratio of 200:1 versus apoA1 for 5 min at 37°C, as previously described (15).

### SANS experiment

Small-angle neutron scattering experiments were carried out at the instrument D22 of the Institut Laue-Langevin, Grenoble, France, and KWS1 at Jülich Center for Neutron Sciences, Garching, Germany. D22 and KWS1 are classical pinhole cameras that provide a high neutron flux. Data were collected for ~2 h from two positions of the detector at the D22 instrument (2 and 5.6 m with collimation lengths of 2.8 and 5.6 m), and three positions of the detector at the KWS1 instrument (1, 2, and 8 m with collimation lengths of 4 and 8 m), and covered a range of momentum transfer ($q$) from 0.008 $Å^{-1}$ to 0.5 $Å^{-1}$. The wavelength λ of the neutron beam used was 6 Å on D22 and 4.5 Å on KWS1. SANS with contrast variation was used to individually map the protein and lipid components in $nHDL_{DMPC}$. The samples were measured at 6–8°C in 12% ($q$ range 0.005–0.304 $Å^{-1}$) and 42% $D_2O$ solution ($q$ range 0.007–0.453 $Å^{-1}$). The radius of gyration ($R_g$) was obtained based on the Guinier approximation (36) from the corresponding scattering curves.

The SANS data collected were processed as follows. The program GNOM (37) was used to deconvolute the scattering intensity curves into the distance distribution function P(R). Subsequently, the program DAMMIN (38) was used to produce low-resolution models (n = 32) of the protein component from the P(R) function obtained for the sample measured in 12% $D_2O$ ($q$ range 0.005–0.256 $Å^{-1}$). The P(R) function obtained from the 42% $D_2O$ scattering intensity curve ($q$ range 0.007–0.453 $Å^{-1}$) was similarly used to obtain low-resolution structures (n = 16) of the lipid component. For some experiments, protein shape was visualized in samples measured at 12% contrast (12% $D_2O$). For these studies, the scattering intensity of the protein was enhanced by preparing nHDL with deuterated apoA1. Both SANS at multiple levels of contrast and mass spectrometry studies independently confirmed that 70% of the nonexchangeable H atoms were substituted by D atoms during protein expression in $D_2O$ with deuterated nutrients, which corresponds to a level of contrast of 92% $D_2O$. Using this information, calculations indicate that, under the conditions employed, the lipid phase (both head groups and acyl chains) contributed <7% of the intensity across all scattering angles examined in the 12% contrast experiment (supplementary Fig. I). We established this value by calculating contributions to intensity coming from the protein and lipid using a modification of the SASSIM program (39). The modification included splitting the total squared scattering amplitude into contributions assigned to various components of HDL (i.e., protein, PC head groups, and PC acyl chains). The contributions to intensity can be either positive or negative, a fact that reflects scattering interference between components. Similar calculations in the 42% contrast experiment, where $HDL_{DMPC}$ is formed with nondeuterated apoA1, indicate the protein component contributes <7% to the total intensity across all scattering angles examined.

### Cross-linking mass spectrometry experiments on reconstituted $nHDL_{DMPC}$ and $nHDL_{DMPC+Chol}$ particles

Chemical cross-linking of apoA1 within $nHDL_{DMPC}$ and $nHDL_{DMPC+Chol}$ was performed by dissolving bis(sulfosuccinimidyl) suberate (BS3) cross-linker (Pierce, Rockford, IL) at 5 mg/ml in 20 mM sodium phosphate buffer, pH 7.4 and immediately adding to 1 mg/ml nHDL in PBS, pH 7.4 at a molar ratio of 200:1. The resulting solution was incubated at 4°C for 24 h with constant gentle mixing. The reaction was quenched by the addition of Tris at a final concentration of 50 mM for 15 min. The resulting cross-linked apoA1 solutions were split into aliquots, digested with sequencing grade chymotrypsin (Promega, Madison, WI) at a ratio of 1:100 (w/w) for 16 h at 25°C, and then stored at 4°C. Cross-linked and chymotrypsin-digested peptides were concentrated with strong-cation exchange (SCX) chromatography using HIL-SCX.25 UltraMicro Tip Columns (Nest Group, Southborough, MA). The samples were prepared for SCX chromatography by adding acetonitrile (5% v/v final) to the cross-linked peptide solution and adjusting to pH 3.0 with $H_3PO_4$ prior to being loaded onto the columns. The column was washed with PBS, pH 3.0 and eluted with 5% acetonitrile, 20 mM sodium phosphate buffer, pH 3.0 with steps of 300 and 500 mM NaCl. A FASTA database of potential cross-linked peptides of apoA1 was generated using the program xComb v1.3 (40). The Uniprot FASTA for apoA1 was used as the input file and the parameters for the database generation included two potential missed cleavages, both intra- and interprotein cross-links, amine to amine cross-linker, no missed cleavage necessary, and a minimum peptide length of four amino acids. Concentrated cross-linked peptides were loaded onto an IntegraFrit sample trap (ProteoPep C18, 300 Å, 150 μm × 2.5 cm; New Objective, Woburn, MA) with 5% acetonitrile in 0.1% formic acid in order to desalt the samples. The peptides were subsequently eluted through a PicroFrit column (75 μm × 15 cm; New Objective) packed in-house with XperTek 218TP, C18, 300 Å pore size, 150 μm particle size (Cobert Associates, St. Louis, MO) using a Proxeon Easy-nLC II system (Thermo Scientific, Waltham, MA) with a gradient of 5–65% acetonitrile, 0.1% formic acid over 120 min into an Orbitrap Velos mass spectrometer (Thermo Scientific). The initial MS screening experiment involved programming the Orbitrap MS to

collect in a data-dependent mode and analyzing the data using the xComb FASTA database in Proteome Discoverer 1.1 (Thermo Scientific) to find precursor masses of potential cross-links. Observed monoisotopic masses within 5 ppm of the theoretical mass of cross-linked peptides of interest were collated into a "parent list" and the Orbitrap MS was programmed to specifically search for the peptides in this list and perform CID MS/MS on the specific peptides. The subsequent MS/MS analyses using the parent list utilized the same chromatographic method as detailed above in the screening experiment. The fragmentation patterns of the resulting data were inspected and assigned manually using Protein Prospector with a signal tolerance of 0.5 Da for the fragment ions (41).

### Hydrogen-deuterium exchange mass spectrometry experiments on reconstituted $nHDL_{DMPC}$ particles

ApoA1 in $nHDL_{DMPC}$ was subjected to hydrogen-deuterium exchange (HDX) at 4°C and at a pH of 7.4 in PBS for various time intervals: 0.5, 1, 2, 75, and 167 min. The reaction was quenched by acidification and by reducing the temperature to 0°C in an ice/water bath. Proteins were subjected to rapid proteolytic digestion using pepsin and immediately injected into an LC-MS system consisting of binary LC20 UPLC pumps (Shimadzu, Kyoto, Japan) and an LTQ ion-trap mass spectrometer (Thermo Scientific). The gradient for elution of the peptides started at 200 μl/min of 0.5% formic acid for 1 min to flush the PBS from the system and then stepped down to 50 μl/min of 10% acetonitrile, 0.5% formic acid and continued to 50% acetonitrile, 0.5% formic acid over 10 min. The trap column consisted of an Everest 238 CV C18 guard column (2.1 mm diameter, Grace, Deerfield, IL) and the analytical column was a Vydac 238TP C18 guard column (2.1 mm diameter, Grace). The resulting spectra were manually interpreted.

### Computational modeling of $nHDL_{DMPC}$

In earlier SANS with contrast variation studies (15, 27) we matched computational models of HDL at multiple contrast levels (0, 12, 42, and 90% $D_2O$) and established that two contrast levels (12 and 42% $D_2O$) are sufficient to produce a consistent model for the entire particle. Thus, thirty-two low-resolution structures obtained from the 12% contrast SANS dataset were averaged, and the SANS shape closest in features to the average shape (reference shape) was further used for modeling. The all-atom model of $nHDL_{DMPC}$ was constructed by separately fitting an all α-helix apoA1 dimer into the reference low-resolution shape envelope, and by packing 160 DMPC molecules into the low-resolution structure of the lipid component (42% contrast SANS dataset, that was similarly averaged, and reference shape used for modeling). Additional constraints were imposed on the lipid packing in the sense that care was taken that lipids from the periphery of the lipid phase that face the apoA1 dimer were arranged such that their acyl chains faced the hydrophobic surface of the protein. Thus, most of lipids were arranged as a bilayer with the exception of about one quarter of them located in between the N/C-termini that form a half-micelle, which connects the two leaves of the bilayer.

The partitioning of the hydrophobic/hydrophilic surface of the apoA1 dimer in $nHDL_{DMPC}$ was determined using "patch" hydrophobicity, which identifies an average per residue hydrophobic index [range (0,1)] calculated by averaging the hydrophobic indices of neighboring amino acid residues located on the same side of the protein (i.e., either facing the solvent or the lipid) in a certain cutoff distance (here the cutoff distance used was 15 Å). The resulting model was further refined by gradually adjusting the conformation of apoA1 chains and lipids until the scattering intensities calculated with CRYSON (42) matched the experimental data. Atom clashes in the all-atom model, which resulted from manual adjustment of chain residues and individual lipid molecules, were removed by performing a short geometry optimization in vacuum. The CHARMM22 force field was used for protein (43), and CHMARMM27 for lipids (44).

The vacuum model of $nHDL_{DMPC}$ was further solvated in a box of TIP4P water molecules (45), with walls 15 Å away from the particle. Sodium ions were added to compensate the negative charge of the two apoA1 chains, and then NaCl ion pairs were inserted to obtain a physiological salt concentration of 344 milliosmolar (standard PBS buffer). The solvated system was energy minimized [using the program GROMACS (46)]. The protocol for geometry optimization was as follows: the lipoprotein particle relaxed gradually (first the solvent, then the lipid, and finally the protein). In the last step of energy minimization all atoms relaxed. Potential energy calculations took into account periodic boundary conditions for the solvated particle. The evaluation of short-range (van der Waals) interactions used a 10 Å cutoff, while Coulomb interactions were calculated using the Ewald summation [Particle Mesh Ewald summation (47, 48)].

SANS decomposition analysis of the lipid core was carried out after splitting the lipid phase into lamellar and micellar domains by visual inspection. The scattering intensities for the whole range of scattering angles were calculated for each individual lipid subdomain. The individual scattering intensity curves were scaled such that the sum of the intensities at zero scattering angle, coming from the two lipid subdomains, equal the intensity at zero scattering angle given off by the entire lipid phase. The scaling procedure is justified by the fact that the intensity at zero scattering angle is proportional to the molecular mass of the lipid (i.e., with the number of lipids in the phase) (49). Of note, this decomposition scheme does not take into account the constructive/destructive interference between the two lipid subdomains. Strictly speaking, only the amplitudes are additive (50). Still, the decomposition scheme is capable of giving insight into the scattering contributions of different subdomains of the lipid phase that are distinguished by different packing characteristics (lamellar vs. micellar).

### Electron microscopy studies

Negative stained nHDL samples (dilution 1:300) were obtained by applying them to the clear side of the carbon-mica interface and staining with 2% (w/v) uranyl acetate. Images were recorded under low-dose conditions with a CM12 (Philips) electron microscope equipped with an LaB6 filament and working at 120 kV. Images have been recorded on an Orius SC1000 CCD camera (Gatan Inc.).

The experimental SANS intensities, the Protein Data Bank files of the SANS shapes for the protein and lipid components of nHDL examined, and the all-atom Turtle model of $nHDL_{DMPC}$ can be downloaded from the site http://www.lerner.ccf.org/cellbio/hazen/data/.

## RESULTS AND DISCUSSION

### Biochemical characterization of nHDL preparations formed using native human apoA1 and perdeuterated human apoA1

Reconstituted nHDL particles generated for SANS analyses in the present study were prepared with either isolated human apoA1 or recombinant human perdeuterated apoA1, as described under Materials and Methods. Before

proceeding with SANS analyses of $nHDL_{DMPC}$ and $nHDL_{DMPC+Chol}$ preparations, particles were extensively characterized. SDS-PAGE and native gel analyses of nHDL forms generated using human apoA1 and deuterated apoA1 showed relatively homogeneous particle preparations (**Fig. 1A, B**). Chemical composition analyses confirmed that the final particle compositions were in close alignment with the initial 80:1, mol:mol (DMPC:apoA1), and 10:80:1, mol:mol:mol (cholesterol:DMPC:apoA1) composition of the DMPC:apoA1 used for particle formation (DMPC:apoA1 of 78.4 ± 2.0:1 and 81.7 ± 3.2:1, mol:mol, for $nHDL_{DMPC}$ generated using human apoA1 and deuterated apoA1, respectively; and cholesterol: DMPC:apoA1 of 8.7 ± 0.2:86 ± 1.7:1, mol:mol:mol, for $nHDL_{DMPC+Chol}$). As expected, cross-linking studies were consistent with all nHDL particle preparations formed containing an apoA1 dimer (Fig. 1C). These $nHDL_{DMPC}$ and $nHDL_{DMPC+Chol}$ preparations were used for all SANS analyses.

As detailed below, all initial studies focused on $nHDL_{DMPC}$ particles. Negative staining of electron microscopy images of the $nHDL_{DMPC}$ formed from either human apoA1 or deuterated apoA1 are shown in Fig. 1D and Fig. 1E, respectively. The images show relatively homogeneous ellipsoidal particles of similar dimensions whether native or deuterated apoA1 was used in $nHDL_{DMPC}$ formation. Approximate overall dimensions of the $nHDL_{DMPC}$ are also shown (Fig. 1D, E; insets of the micrographs).

### SANS studies reveal that the low-resolution structure of apolipoprotein A1 within $nHDL_{DMPC}$ is an open and slightly out of plane shape with three arms

To directly visualize the shape of apoA1 within $nHDL_{DMPC}$, particles were analyzed by neutron scattering at 12% contrast (12% $D_2O$). Under these conditions the average scattering length density of the lipid component matches the scattering properties of the solvent at zero scattering angle and is thus "invisible". The selective deuteration of the protein further intensifies the scattering signal from the protein, making it possible to minimize (<7%, supplementary Fig. I) the contribution of the lipid to the intensity at higher scattering angles, thus allowing the use of the low-resolution shape obtained at 12% contrast to serve as a scaffold for constructing a model for the protein conformation. Initial SANS data collected during the 12% contrast variation study of the protein component of $nHDL_{DMPC}$ were used to construct 32 low-resolution structures for apoA1 in $nHDL_{DMPC}$ as described under Materials and Methods. All demonstrated similar essential structural features for apoA1, a shape with three distinct arms. Supplementary Fig. II includes a random sampling of 15 of the 32 low-resolution shapes, along

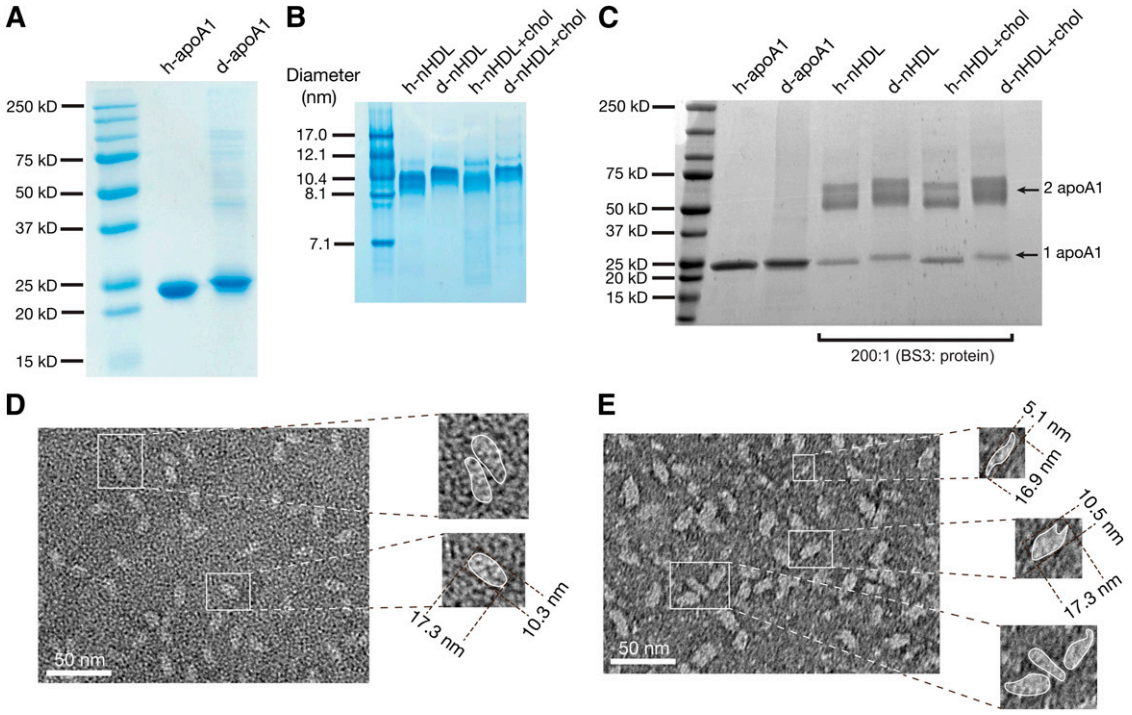


**Fig. 1.** Particle composition analyses. A: SDS-PAGE gel of human (h)-apoA1, and perdeuterated (d)-apoA1. B: Nondenaturing gel of $nHDL_{DMPC}$ and $nHDL_{DMPC+Chol}$ particles reconstituted with h-apoA1 (h-nHDL) and d-apoA1 (d-nHDL). C: Cross-linking gel shows that h-nHDL and d-nHDL with and without cholesterol preparations contain two apoA1 chains per particle. D: Electron microscopy (EM) negative staining of $nHDL_{DMPC}$ preparations reconstituted with h-apoA1. The insets show magnified areas of the EM micrograph in which the contour of the particles has been marked with a white boundary line to compensate for the decrease in contrast resulting from magnification. The overall dimensions of the particles match those obtained from the low-resolution structure of $nHDL_{DMPC}$. E: Negative staining EM of $nHDL_{DMPC}$ preparations reconstituted with d-apoA1. Similarly, insets show magnified particles. Of note, the top inset identifies an $nHDL_{DMPC}$ particle in an orientation that exposes the side of the particle with a thickness similar to the apoA1 chains.

with an average shape calculated from all of the low-resolution shapes. Because the scattering intensities predicted from the average shape do not agree as well with the experimental data ($\chi^2$ = 5.42) as that calculated for each of the individual low-resolution shapes ($\chi^2$ < 0.85 for each), the low-resolution shape that most closely resembled the average shape was selected as the reference shape (supplementary Fig. II), and was then used to build a cartoon of the apoA1 double chain (vide infra), as described under Materials and Methods. The experimental scattering intensities obtained at various scattering angles (**Fig. 2A**), and the intensities collected at very small scattering angles (Fig. 2B) were used to determine the radius of gyration according to Guinier approximation (36). Figure 2C portrays the distance distribution function, P(R), which constitutes a fingerprint for the specific conformation of the protein (37). Deconvolution of the scattering intensities from the 12% contrast SANS experiments reveals a low-resolution structure (resolution 24 Å) of protein (also known as apoA1 dimer) within $nHDL_{DMPC}$, as illustrated in Fig. 2D. The average thickness of the apoA1 double chain is 22–24 Å. So at the SANS resolution of the protein component we cannot distinguish the individual chains (as actually shown by the SANS shape),

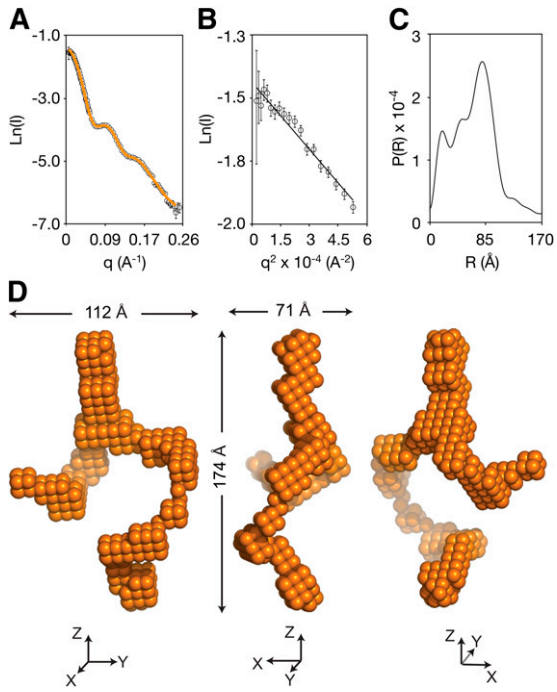


**Fig. 2.** $nHDL_{DMPC}$ in 12% $D_2O$. A: Logarithm of the scattering intensity versus the scattering vector, *q*. The curve displays maxima and minima, which are a result of constructive and destructive interferences produced by the conformation of apoA1 chains in $nHDL_{DMPC}$. B: The Guinier plot was used to determine the radius of gyration. C: The distance distribution function, P(R), was obtained by the deconvolution of the scattering intensities. P(R) constitutes a fingerprint for apoA1 architecture in $nHDL_{DMPC}$, and was used to produce the low-resolution structure of the protein component of $nHDL_{DMPC}$. D: The low resolution structure of the protein component of $nHDL_{DMPC}$ in various orientations. The overall dimensions of the low resolution structure are shown, which are in excellent agreement with dimensions obtained from EM.

but we can resolve the shape of the double chain. To build a molecular model of apoA1 in $nHDL_{DMPC}$ we used information about the composition (number of apoA1 chains per nHDL particle) and alignment of the two chains with respect to each other, that is, the antiparallel orientation and the registry based on multiple published Lys-Lys proximity distances as probed by cross-linking mass spectrometry experiments. Notably, the protein shape is distinct from a classic "belt" configuration. Rather, the protein envelope visualized has three distinct arms, is open, and follows a contorted shape with two arms clearly out of plane. Measured parameters for the protein component of $nHDL_{DMPC}$ include a radius of gyration ($R_g$) of 52.4 Å, and overall outer dimensions of approximately 174 × 112 × 71 Å (Fig. 2D, **Table 1**). The scattering intensities calculated from the low-resolution protein envelope nicely overlay the experimental scattering data (Fig. 2A), and show an excellent statistical fit with experimental scattering intensities (root mean square deviation, $\chi^2$ = 0.82; Table 1).

### The low-resolution structure of the lipid component of $nHDL_{DMPC}$ has an oblate ellipsoidal shape

To visualize the low-resolution structure of the lipid phase of $nHDL_{DMPC}$ we performed contrast variation SANS studies in 42% $D_2O$ on $nHDL_{DMPC}$ particles reconstituted with nondeuterated apoA1. At this $D_2O$ concentration, the scattering length density of the solvent matches that of the nondeuterated protein at zero scattering angle; thus, the scattering signal measured arises mostly from the lipid phase of the lipoprotein and at higher scattering angle calculations indicates that the protein contributes <7% to the total intensity (see Materials and Methods). The scattering intensities, the Guinier range, and the distance distribution function P(R) of the lipid component of $nHDL_{DMPC}$ are shown in **Fig. 3A–C**. Deconvolution of the scattering data yields an oblate ellipsoid. Sixteen shapes were averaged (Materials and Methods, supplementary Fig. III), and a reference shape that best interlocked with the protein shape was selected as reference shape, which had dimensions 88 × 76 × 52 Å (Fig. 3D). The calculated scattering intensities from the low-resolution shape envelope of the $nHDL_{DMPC}$ lipid phase are in excellent agreement with the experimental data (Fig. 3A, Table 1; $\chi^2$ = 2.29). On a cautionary note, we remark that the SANS studies by themselves lack the resolution to determine details of molecular packing of indivudual lipids within the particle (e.g., lamellar vs. micellar vs. other smectic mesophase), but further decomposition analysis of the intensities may actually provide further understanding of lipid packing in HDL (vide infra).

Overlays of the low-resolution structures of both protein (orange) and lipid (green) components of $nHDL_{DMPC}$ are shown in Fig. 3E. The lipid shape matches the protein shape like a key in a lock, with the overall low-resolution structure of the $nHDL_{DMPC}$ particle resembling a "turtle", so from now on we will refer to the structural model of $nHDL_{DMPC}$ generated from 80:1, DMPC:apoA1 as the "Turtle model".

TABLE 1. Radius of gyration, global dimensions, and goodness of fit of the Turtle model of $nHDL_{DMPC}$ with experimental SANS data

| | Radius of Gyration[a] (Å) | | Dimensions (Å) | $\chi^{2a,b}$ | |
|---|---|---|---|---|---|
| Model | Protein | Lipid | L × W × H | Protein[a] | Lipid[a] |
| Experimental:[c] | | | | | |
| $nHDL_{DMPC}$ | 52.4 | 30.4 | — | — | — |
| $nHDL_{DMPC+Chol}$ | 50.7 | 33.5 | — | — | — |
| SANS shapes: | | | | | |
| $nHDL_{DMPC}$ | 51.4 | 30.3 | 174 × 112 × 82 | 0.840[d] | 2.291[d] |
| $nHDL_{DMPC+Chol}$ | 50.8 | 35.4 | 114 × 113 × 56 | 0.880[d] | 0.950[d] |
| EM[e] | | | 173 × 105 × 51 | | |
| Turtle model | 52.0 | 30.2 | 175 × 103 × 62 | 0.985[f] 1.103[g] | 2.309[f] 3.646[g] |
| Belt model[h] | 48.7 | 29.9 | 106 × 106 × 22[i] | 5.436 | 7.458 |
| 1AV1[j,k] | 48.9 | — | 126 × 89 × 52[i] | 4.024 | — |
| Saddle-1 model[k] | 48.9 | — | 104 × 104 × 48[i] | 5.306 | — |
| Saddle-2 model[k] | 46.4 | — | 101 × 92 × 58[i] | 4.455 | — |
| Saddle-3 model[k] | 44.9 | — | 91 × 91 × 63[i] | 7.292 | — |
| Saddle-4 model[k] | 41.4 | — | 80 × 80 × 73[i] | 12.790 | — |

Radius of gyration ($R_g$) and overall dimensions of the low resolution structures (SANS shapes) and the Turtle, Belt, and Saddle models of $nHDL_{DMPC}$. Calculated $\chi^2$ statistics (root mean square difference), that quantify differences between experimentally determined scattering intensities (measured by SANS with contrast variation) and theoretically calculated, show a better fit for the Turtle model compared with the Belt or various Saddle models of apoA1 dimer. EM, electron microscopy.

[a]Calculated with CRYSON.

[b]The root mean square difference between the calculated and experimental scattering intensities.

[c]Calculated with GNOM from experimental scattering intensity using the Guinier approximation.

[d]Calculated with DAMMIN.

[e]Particle dimensions of $nHDL_{DMPC}$ from negative staining EM images (see Fig. 1).

[f]A short energy minimization in vacuum was performed with GROMACS for each component (protein and lipid) individually (see Materials and Methods).

[g]Full energy minimization in solution was performed with GROMACS for the $nHDL_{DMPC}$ model (see Materials and Methods).

[h]Supplementary Fig. VIII.

[i]Protein component only.

[j]The crystal structure of lipid-free truncated (Δ43) apoA1 dimer.

[k]Supplementary Figs. XII and XIII (15).

### ApoA1 within $nHDL_{DMPC}$ has an open conformation with a large hairpin and N/C-termini folded back

Having the low-resolution structure of the protein component of $nHDL_{DMPC}$ generates a puzzle in how to fit an apoA1 dimer within the observed protein shape. The known crystal structures of lipid-free apoA1 truncated mutants (19, 20), and the preponderance of structural data on nHDL particles (11, 12, 14, 15, 21, 22) argue that the two apoA1 chains are oriented in an antiparallel fashion. We therefore sought to develop a hypothetical three-dimensional model of the apoA1 antiparallel dimer that fit within the constraints of the low-resolution protein structure (**Fig. 4**). First, direct visualization of the overall shape envelope suggests only a few global configurations (in the crude sense) of how an apoA1 dimer can be arranged such that its full length fits within the protein shape envelope experimentally visualized. Closer inspection of the three "arms" (Fig. 4A*a–c*) of the protein shape envelope reveals that the approximate cross-sectional area of two arms (Fig. 4A*a*, *c*, each ~120 $Å^2$) are roughly the dimensions predicted by two classic α-helices (~65 $Å^2$ each, including residue side chains), whereas the third arm (Fig. 4A*b*) appears to be substantially (~2-fold) larger (~234 $Å^2$). We therefore chose to entertain an apoA1 configuration where the dimeric chains fold upon themselves forming a hairpin that fills arm *b*, leaving the other two arms to contain the N- and C termini (Fig. 4).

To help build a three-dimensional model of the apoA1 dimer, we traced the protein shape envelope with two tubular pathways, one for each monomer, each tube having the anticipated cross-section of a classic amphipathic α-helix (not including side chains). These "pipes" are gradient colored (dark → light, N terminus → C terminus) in red and blue (for the two apoA1 chains), and are superimposed in an antiparallel orientation onto the low-resolution protein structure of $nHDL_{DMPC}$ in Fig. 4A. Next, we built conformations of the two apoA1 monomers that matched the tube paths and maintained proper orientation of the hydrophobic/hydrophilic face of the amphipathic helical surfaces taking into account the presumed location of the lipid core of the particle. Following energy minimization, the crude proposed three-dimensional model obtained for the apoA1 chains within $nHDL_{DMPC}$ is shown in Fig. 4B (stereo views in supplementary Fig. IV), and its superposition onto the low-resolution structure of apoA1 is given in Fig. 4C. It should be noted that this hypothetical exercise was done not to claim that this was the precise structure of apoA1 within $nHDL_{DMPC}$, but rather, to help build a model that displayed overall architecture that matched the experimental data collected by the SANS studies, and would then likely also match previously reported MS cross-linking, ESR, and FRET data on reconstituted nHDL particles (11, 12, 15, 21, 22).

To assess the goodness of fit of the protein component of the Turtle model with the experimentally determined

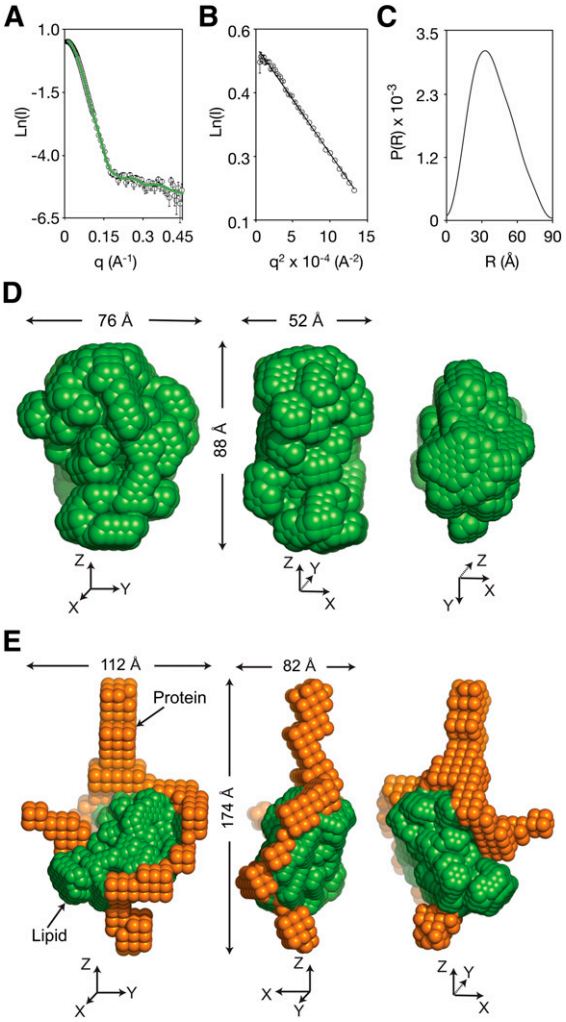


**Fig. 3.** $nHDL_{DMPC}$ in 42% $D_2O$. A: Logarithm of the scattering intensity versus the scattering vector, *q*. B: The Guinier plot. C: The P(R) function is characteristic to an oblate ellipsoid; the function is smooth without additional decorations as the function for the protein component. D: The low-resolution structure of the lipid component of $nHDL_{DMPC}$ is shown in various orientations; the shape is not discoidal, rather asymmetric but flattened as an oblate. E: Overlap of the low-resolution structures. The protein component (orange, 12% $D_2O$) is superimposed on the lipid component (green, 42% $D_2O$) of $nHDL_{DMPC}$. The two low-resolution structures fit as a "key in a lock". The composite low-resolution structure of $nHDL_{DMPC}$ shows that a significant domain of the protein is not adjacent to the lipid phase, while the lipid phase is not entirely enshrined by the protein component.

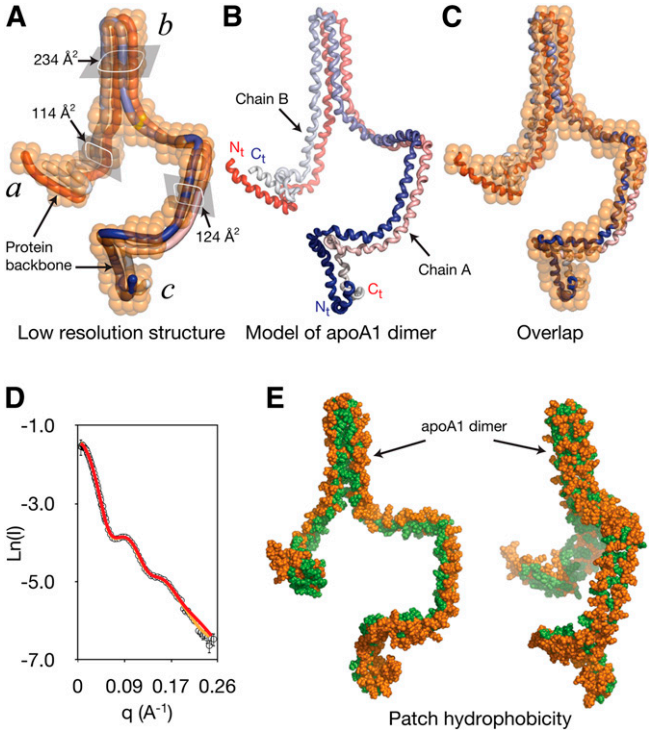


**Fig. 4.** Model of apoA1 dimer in $nHDL_{DMPC}$. A: Tube representation of the apoA1 dimer superimposed on the low resolution structure of nHDL in 12% $D_2O$ (orange). The tubes correspond to the two chains of apoA1 dimer and are gradient colored with red and blue. Approximate calculated cross-sectional areas in each arm (*a*, *b*, and *c*) of the low resolution structure are also shown. B: Hypothetical three-dimensional model of apoA1 dimer represented as a continuous helix. The two chains of apoA1 are gradient colored with red and blue, with the N termini colored in red/blue and C termini colored in light red/blue. C: Overlap of the low-resolution structure with the protein model. D: Superposition of the experimental neutron scattering intensities (12% $D_2O$, open circles with error bars) with the scattering intensities calculated from the protein model (red line) and the low-resolution structure of $nHDL_{DMPC}$ in 12% $D_2O$ (orange). E: Patch hydrophobicity of the residues in apoA1 of $nHDL_{DMPC}$. Patch-hydrophilic residues are colored orange and patch-hydrophobic residues are colored in green.

scattering data (12% contrast), predicted scattering intensities were calculated. They showed excellent statistical fit with experimental scattering intensities (root mean square difference, $\chi^2 = 0.985$; Table 1, Fig. 4D). To assess the orientation of the hydrophobic/hydrophilic residues in the amphipathic protein within the Turtle model, we calculated the patch hydrophobicity [15 Å (14)], since this would better reflect the predicted overall amphipathic partitioning of side chains on the apoA1 dimer. Visual inspection (Fig. 4E; hydrophilic residues orange, hydrophobic residues green) confirmed that the residues in the protein model had orientations in accord with a typical amphipathic peptide, with the green (hydrophobic) surface clearly oriented toward the cavity wherein the lipid core resides. Also notable is that the hydrophobic surfaces of the amphipathic helices abut one another within the hairpin in arm *b* (Fig. 4E), allowing for protection from the aqueous phase. Of note, many of the hydrophobic residues in the N- and C-terminal regions of apoA1 that are not associated with phospholipids are not predicted to be exposed to aqueous solvent because of being shielded by the protein fold (i.e., hydrophobic-hydrophobic interactions of amphipathic α-helical surfaces) in these regions (Fig. 4E). Further, the large hairpin houses residues (e.g., $R_{149}$, $R_{153}$, and $R_{160}$) on one apoA1 chain previously identified as being important in LCAT activation (51).

### Mass spectrometry cross-linking studies provide independent experimental data confirming the existence of a large hairpin domain of apoA1 in $nHDL_{DMPC}$

We sought to obtain independent experimental data directly supporting the finding that a significant domain of

apoA1 within $nHDL_{DMPC}$ particles is folded onto itself in a large hairpin. Using the Turtle model of $nHDL_{DMPC}$ and a 12 Å distance for the BS3 bifunctional cross-linking agent, we predicted in silico that up to 15 Lys-Lys cross-links (both intrachain and interchain) might exist in the predicted hairpin domain of ApoA1. Nevertheless, none of the postulated cross-links predicted have yet to be identified in other reported cross-linking studies of HDL preparations (N.B. no MS cross-linking studies are reported yet for a 1:80 (mol:mol), apoA1:DMPC HDL particle). Remarkably, using the exact mass of the proposed cross-links (see Materials and Methods for experimental approach), we were able to experimentally identify (using 5 ppm tolerance) all 15 cross-links by high-resolution mass spectrometry, and among these, eight were sequence confirmed by MS/MS (**Fig. 5**). For illustrative purposes, supplementary Fig. V shows the full scan MS/MS spectrum of cross-link $Lys_{59}$-$Lys_{133}$, which along with cross-link $Lys_{133}$-$Lys_{195}$, spans the base of the hairpin and affirms the large size of the hairpin (~50 Å).

### HDX tandem mass spectrometry studies provide additional independent confirmatory data in support of a distinct environment for apoA1 regions within the hairpin

Numerous studies support the antiparallel orientation of the two apoA1 chains within nHDL with a defined registry [similar to that observed for the crystal structure of lipid-free apoA1 (19, 20) ]. Indeed, this registry for the two antiparallel apoA1 chains is needed to accommodate the many distance constraints obtained from multiple biophysical approaches including cross-linking mass spectrometry (11, 15, 21, 22), electron spin resonance spectroscopy (12), and fluorescence resonance energy transfer (12, 52) studies. When incorporating the antiparallel apoA1 chains within the Turtle model, care was taken to retain this predicted registry. Closer inspection of the Turtle model suggests that specific regions of apoA1 within the hairpin on one chain would not be predicted to be within the hairpin on the antiparallel apoA1 chain (**Fig. 6**). We therefore performed HDX kinetic analyses, which are sensitive to the local environment, on three apoA1 peptides in $nHDL_{DMPC}$ particles ($Y_{115}$-$L_{126}$, $L_{159}$-$L_{170}$, and $R_{171}$-$L_{178}$) that are predicted to be located in the hairpin domain of one chain, but not of the other. Thus, we hypothesized that these peptides might demonstrate evidence of two distinct environments, such as the presence of bimodal kinetics when examining the rates of H/D exchange within amide protons in these sequences. The kinetic curves for the three peptides (percent of deuterium incorporation vs. HDX time) are shown in supplementary Fig. VI. Remarkably, each showed readily detectable bimodal kinetics (presence of both a slow and a fast exchanging peptide) for deuterium buildup rates, consistent with the presence of at least two distinct environments for these apoA1 sequences within the $nHDL_{DMPC}$ particles. The slow-exchanging peptides had rate constants approximately two orders of magnitude lower than that predicted for random-coil peptides having the same sequence. Conversely, we observed

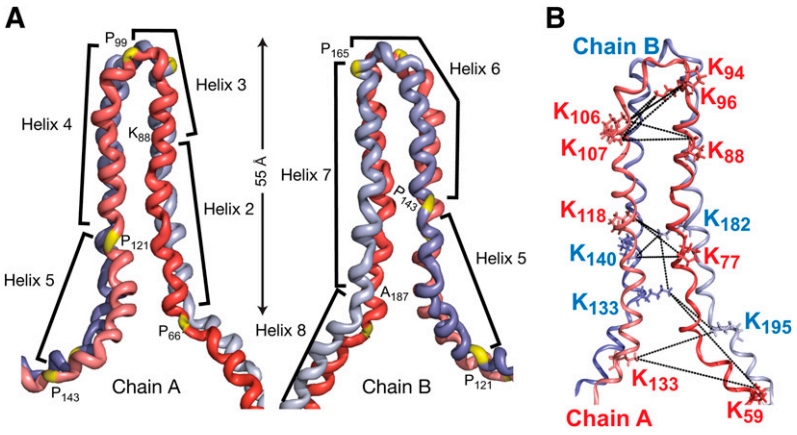


| | Peptide$_1$ | Peptide$_2$ | Δppm[1] | Dist (Å)[2] |
|---|---|---|---|---|
| $K_{59}$-$K_{133}$ | RAELQEGARQKL | DSVTSTFSKL | 3.57 | 27.6 |
| $K_{59}$-$K_{133}$ | RAELQEGARQKL | DSVTSTFSKL | 3.57 | 28.4 |
| $K_{77}$-$K_{118}$ | YRQKVEPL | DNLEKETEGL | 1.20 | 14.2 |
| $K_{77}$-$K_{140}$ | HELQEKL | EKETEGLRQEM*SKDL | 0.044 | 14.2 |
| $K_{88}$-$K_{106}$ | QKKWQEEMEL | RQEMSKDL | 0.038 | 14.3 |
| $K_{88}$-$K_{107}$ | QKKWQEEMEL | RQEMSKDL | 0.038 | 14.7 |
| $K_{94}$-$K_{106}$[3] | EEVKAKVQPYL | QKKWQEEMEL | 4.934 | 13.1 |
| $K_{94}$-$K_{107}$[3] | EEVKAKVQPYL | QKKWQEEMEL | 4.934 | 9.2 |
| $K_{96}$-$K_{106}$[3] | EEVKAKVQPYL | QKKWQEEMEL | 4.934 | 17.3 |
| $K_{96}$-$K_{107}$[3] | EEVKAKVQPYL | QKKWQEEMEL | 4.934 | 19.0 |
| $K_{118}$-$K_{182}$ | RQKVEPLRAEL | EALKENGGARL | 0.973 | 10.4 |
| $K_{133}$-$K_{182}$ | KENGGARL | QEGARQKLE* | 1.549 | 13.0 |
| $K_{133}$-$K_{195}$[3] | GARQKLHE | YHAKATEHLSTLSE | 0.270 | 18.8 |
| $K_{133}$-$K_{195}$[3] | GARQKLHE | YHAKATEHLSTLSE | 0.270 | 13.5 |
| $K_{140}$-$K_{182}$[3] | KENGGARL | HELQEKL | 0.311 | 8.4 |

[1]Difference between the theoretical and observed crosslinked dipeptide masses
[2]Distance in the molecular model built from the low resolution structure
[3]Not confirmed by MS/MS
M*=oxy-Met; E*=pyro-Glu

**Fig. 5.** The hairpin domain of apoA1 in the Turtle model of $nHDL_{DMPC}$ and cross-links in the hairpin domain. A: At left, the hairpin is shown with the chain A (red) on top. The chain A helices that participate in the formation of the hairpin are helices 2, 3, 4, and 5. At right, the hairpin is shown with the chain B (blue) on top. Helices 5, 6, and 7 from chain B are involved in the formation of the hairpin; proline residues are colored yellow. B: Fifteen predicted cross-links within the hairpin region of apoA1 within the Turtle model for $nHDL_{DMPC}$ were observed by high-resolution MS analyses (within 5 ppm). The sequences of more than half of the predicted cross-links, except where indicated, were identified by MS/MS analyses.

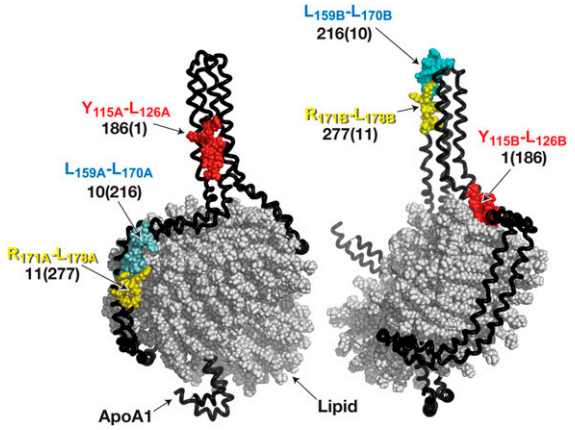


**Fig. 6.** HDX protection factors for three peptides located in the hairpin domain of the Turtle model of $nHDL_{DMPC}$. When peptides $Y_{115}$-$L_{126}$ (red spheres) are located in the hairpin, the peptides $L_{159}$-$L_{170}$ (blue spheres) and $R_{171}$-$L_{178}$ (yellow spheres) in the same protein chain are located outside the hairpin, and vice versa. All three peptides exhibit bimodal H/D exchange that is fast (low protection factor, black) and slow (high protection factor).

that the fast exchanging peptides incorporated deuterium either as fast as their random-coil counterpart in the case of peptide $Y_{115}$-$L_{126}$, or at least one order of magnitude faster than their slow-exchanging counterparts (e.g., peptides $L_{159}$-$L_{170}$ and $R_{171}$-$L_{178}$). Figure 6 shows the location and experimentally determined HDX protection factors of these three peptides ($Y_{115}$-$L_{126}$, $L_{159}$-$L_{170}$, and $R_{171}$-$L_{178}$) on the two apoA1 chains in the Turtle model. Peptides located in the hairpin domain do not interact with lipid, in contrast to their counterparts outside of the hairpin and located on apoA1 domains that interact with lipid. The distinct partitioning of the peptides and corresponding microenvironment (either interacting with the lipid or not) seems to correlate with their H/D exchange behavior, i.e., fast versus slow. Based on our HDX data on the Solar Flare region of apoA1 ($L_{159}$-$A_{180}$), which we found to exchange much faster when bound to lipid than in lipid-free apoA1 (14), we can hypothesize and extrapolate to assume that peptides that experience a protein-protein interaction environment only may demonstrate slower H/D exchange (i.e., higher protection factor), in general, because they may be more tightly packed and less susceptible to unfolding due to the diversity of intermolecular interactions they experience (e.g., charge-charge, charge-dipole, dipole-dipole, and H-bond). On the other hand, peptides interacting with lipids experience only weak van der Waals interactions, which make them more susceptible to unfolding, and thus for exposed amide H, to faster H/D exchange.

It is also noteworthy to mention that we found that the Solar Flare region ($L_{159}$-$A_{180}$), corresponding to peptides $L_{159}$-$L_{170}$ and $R_{171}$-$L_{178}$ on one chain of apoA1 in the $nHDL_{DMPC}$ particle, demonstrated fast H/D exchange (protection factor 10 and 11, respectively) even at 5°C. Thus, our HDX data on $nHDL_{DMPC}$ confirm our earlier result obtained for $nHDL_{POPC}$ (nHDL reconstituted with POPC and cholesterol) (14) that this domain of apoA1 is an unstructured loop and not a helical domain as was inferred indirectly by Sevugan Chetty et al. (24) from their HDX data (5°C) and the overall predicted α-helical content of apoA1 based on circular dichroism data on $nHDL_{POPC}$.

### The lipid domain of $nHDL_{DMPC}$ is predicted to be predominantly lamellar (bilayer) with a small micellar domain

We next sought to further investigate the possible organization of the phospholipids within the lipid core of the $nHDL_{DMPC}$ particles so that eventually, a hypothetical global all-atom model of the particle could be constructed. To build the three-dimensional model of the lipid phase, we used the reference low-resolution structure obtained from the 42% contrast SANS experiments (Fig. 3D, supplementary Fig. III) as the shape envelope within which the phospholipids were placed using the known composition of the particle as a guide for the number of phospholipids to include. Similar to the case of developing the protein model, the manner in which individual lipids might be arranged within the lipid core was not obvious from the SANS data alone. However, the fact that the apoA1 chains within $nHDL_{DMPC}$ have an open conformation, coupled with the known biophysical properties and packing characteristics of phospholipids, provide some logical suppositions to the packing. First, it is presupposed that the lipids within the particle will be organized predominantly as a bilayer domain, in keeping with this lipid organization being stable, a known packing structure for choline glycerophospholipids, and whose dimensions are compatible with the majority of the lipid SANS shape observed. However, the open arms of the apoA1 chains necessitate that a nonlamellar lipid organization occur in these regions, since it logically follows that a domain within the lipid core of the particle will have to accommodate the exposed region to the aqueous surface where the open apoA1 ends fail to overlap and enshrine the lipid (Fig. 4, and see below). What the packing organization of this region is cannot be unequivocally determined with the current data. Nevertheless, the protein shape argues that a smaller micellar domain that caps the space between the open N/C-termini of the apoA1 dimer might occur (Fig. 4A). A final hypothetical all-atom model of the lipid phase was thus obtained by combining a predominantly bilayer organization with a small micellar end-cap domain, followed by energy minimization. The combination of the two arrangements (bilayer and micellar) is evident from the different orientations shown in **Fig. 7**. Figure 7B displays the superposition of the calculated scattering intensities from the hypothetical lipid model and the experimental data, which demonstrated an excellent statistical match ($\chi^2 = 2.31$, Table 1). Visual inspection of the superposition of the hypothetical lipid model developed and the low-resolution SANS structure (42% contrast reference shape envelope for lipid) is shown in Fig. 7C, and is notable for the excellent match. Overlay of the protein and lipid components, followed by energy minimization, yielded the three-dimensional all-atom model of $nHDL_{DMPC}$ (the Turtle model; **Fig. 8**, stereo view in supplementary Fig. VII),

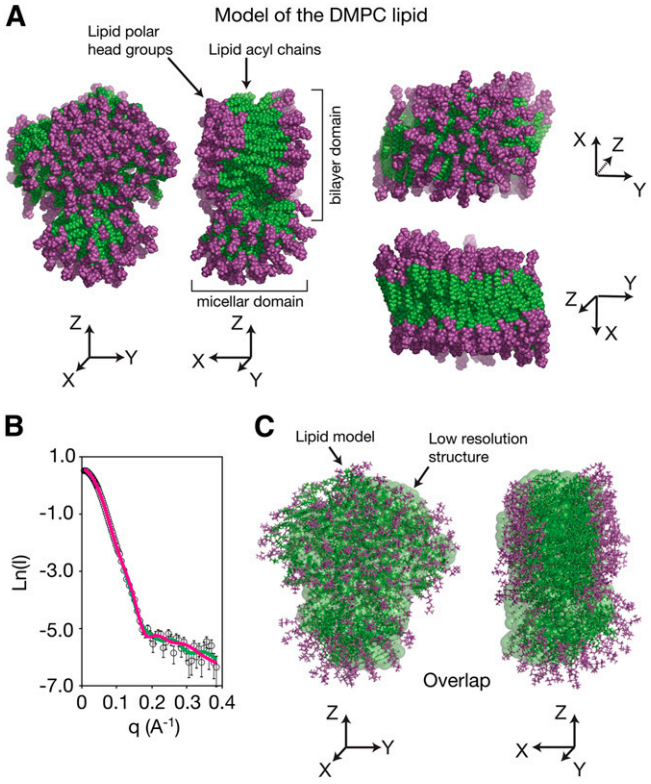


**Fig. 7.** Model of lipid component in $nHDL_{DMPC}$. A: Sphere representation of the lipid component of $nHDL_{DMPC}$ in various orientations. The lipid heads are colored in purple and the acyl chains are colored in green. The second orientation of the lipid model (from the left) shows that the lipid component is a combination of bilayer and micellar domains. B: Superposition of the experimental neutron scattering intensities (42% $D_2O$, open circles) with the scattering intensities calculated from the lipid model (purple line) and the low-resolution structure of $nHDL_{DMPC}$ in 42% $D_2O$ (green). C: Overlap of the low resolution structure of $nHDL_{DMPC}$ obtained in 42% $D_2O$ and the lipid model, in two different orientations.

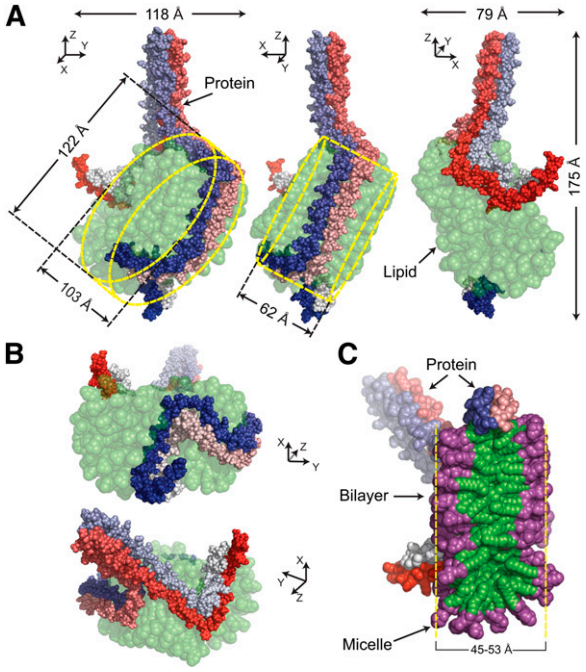


**Fig. 8.** The Turtle model of $nHDL_{DMPC}$. A: Sphere representation of $nHDL_{DMPC}$ in various orientations. ApoA1 chains are colored with gradient color starting dark red/blue for the N termini and ending with light red/blue for the C termini. The lipids are colored in green. B: Two additional orientations of the Turtle model. The top orientation shows the micelle domain of the lipid, while the bottom orientation shows the hairpin made by apoA1 pointing out of plane. C: Cross-section of the Turtle model that shows the partitioning of the lipid into two distinct domains, a bilayer and a micelle. The lipid heads are colored in purple and the acyl chains are colored in green. The thickness of the lipid bilayer agrees well with that obtained from EM.

which will be discussed in detail below. Of note, the overall form is that of a discoidal particle with a protruding hairpin.

### Discussion of the Turtle model in the historical context of prior discoidal models of nHDL

The first proposed discoidal model of nHDL, the bicycle tire micelle (a.k.a., Belt) model (29, 53), was inferred from SANS (without contrast variation) and electron microscopy studies of $nHDL_{DMPC}$ with identical lipid composition to the particle studied herein, but using an N-terminal Δ43 truncated apoA1 mutant. Two decades later, an all-atom model was proposed for $nHDL_{POPC}$ (9) by using the lipid-free crystal structure of apoA1 (19) as a template for the relative orientation of the two apoA1 chains. The Belt model is characterized by a closed double belt conformation of the antiparallel apoA1 dimer encircling a lipid bilayer (9). Virtually all subsequent refinements to models of nHDL (11–14) have posited a closed apoA1 dimer in a belt configuration that completely enshrines a central lipid bilayer, regardless of lipid composition. We recently used SANS with contrast variation to directly visualize for the first time the protein component of nHDL reconstituted with apoA1:POPC:cholesterol (1:100:10, mol:mol:mol) (15). The protein structure revealed in these lipoprotein preparations identified an apoA1 dimer that adopted an open helical shape [DSH model (15)]. Further, when coupled with contrast variation SANS analyses of the lipid components of this nHDL preparation, H/D exchange tandem mass spectrometry results, and biochemical constraints (FRET, ESR, and mass spectrometry cross-linking), the lipid corresponding to this particle (composition 100:10:1, POPC:cholesterol:apoA1) appeared to adopt a micellar/pseudolamellar packing organization. Subsequent multinuclear NMR studies of this particle corroborated this assertion, showing multiple $^{31}P$ NMR spectral features characteristic of a micellar packing organization, and distinct from a lamellar (bilayer) organization (27). It is thus remarkable that the present SANS studies of an nHDL particle generated from the classic starting composition of 80:1 (DMPC:apoA1), both confirmed prior assertions of a predominantly discoidal nHDL particle (generated at this lipid:protein composition), yet also revealed an open apoA1 configuration, and also posits the presence of a nonlamellar (bilayer) domain, presumably a small micellar lipid endcap. Contrast variation SANS allows for direct visualization of the time-averaged conformation of the protein within the particle, and clearly shows an open configuration for the apoA1 dimer (Figs. 2, 4).

And while the SANS studies lack resolution to determine the molecular packing of the lipid within the particle, it logically follows that a domain within the lipid core of the particle will have to accommodate the exposed region to the aqueous surface where the open apoA1 ends fail to overlap and enshrine the lipid (Fig. 4, and see below).

Historically, $nHDL_{DMPC}$ has been used by many [e.g., (16, 17, 29, 33, 54, 55)] to study the structure of nHDL because the shorter fatty acyl chains in DMPC enable large unilamellar vesicles (LUVs) of DMPC to spontaneously associate with apoA1, especially at the transition temperature (23°C) of DMPC vesicles. Despite the ease of formation of these HDL preparations, they also are relatively heterogeneous, with predominantly two sizes of nHDL particles [9.8 nm and 10.4 nm (33)]. In addition, by mixing LUV/DMPC with apoA1 to form nHDL, residual LUVs and free apoA1 also remain (55), making such preparations difficult to study and interpret by SANS, which requires monodispersed samples. Consequently, we used the classic cholate dialysis method for reconstituted nHDL formation with the DMPC in the present studies because we observed that superior (with respect to homogeneity) particle preparations of identical size to the major particles observed with DMPC/LUV:apoA1 mixtures were obtained, that could be purified more readily using size exclusion chromatography prior to SANS analyses (Fig. 1).

### Further analyses of SANS data yield insights into potential lipid packing in $nHDL_{DMPC}$

As noted above, the open protein shape observed from the 12% contrast SANS analyses of $nHDL_{DMPC}$ dictates that some phospholipid within the particle must possess a packing organization different from a simple bilayer. To this end, we sought to determine whether further examination of the 42% contrast SANS data could shed light on the different lipid packing that might exist in this region of the particle. In the Belt model of $nHDL_{DMPC}$ (33) all 160 DMPC lipids make a bilayer (supplementary Fig. VIIIA, B). One can calculate the theoretical scattering intensity given off by such a lipid bilayer (supplementary Fig. VIIIC, solid green line). Examination of this plot reveals that it does not agree well with the experimental data at higher scattering angles (supplementary Fig. VIIIC), while the predicted scattering curve from the lipid core comprised of both lamellar (bilayer) and micellar configurations, as proposed in the Turtle model (Figs. 7, 8), is in excellent agreement with the experimentally determined scattering intensities in the 42% contrast SANS study of $nHDL_{DMPC}$ (Fig. 7B, supplementary Fig. VIIIC).

To further investigate the impact of lipid packing on the predicted SANS scattering data and to better understand the discrepancy in predicted SANS scattering intensities from a purely lamellar (e.g., Belt) versus combined lamellar/micellar (Turtle) model, we examined the individual contributions of the two predicted domains within the Turtle model (**Fig. 9**). An illustration of the different domains within the lipid core of the particle is shown in Fig. 9A, wherein approximately 28% of the lipids form the micellar domain (see also Fig. 9B for different views of the

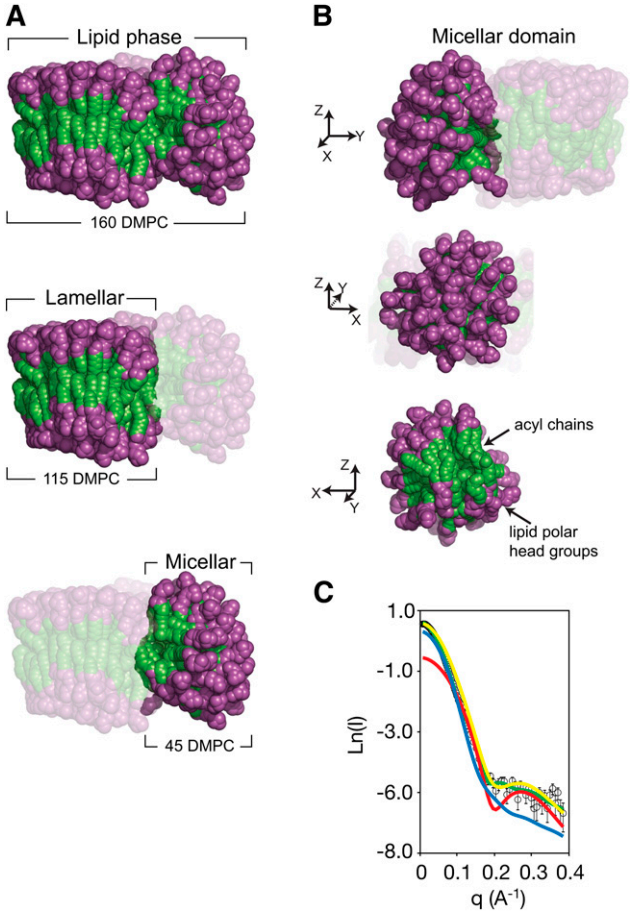


**Fig. 9.** Decomposition of scattering intensities for the lipid model of $nHDL_{DMPC}$. A: Top panel shows the lipid phase of the Turtle model as a mixture of a predominant bilayer and a smaller micelle. The center panel shows the bilayer domain, while the micellar domain is faded. The bottom panel shows the micelle while the lameller domain is faded. The DMPC polar groups are colored purple and the acyl chains are colored green. B: The micellar domain in different orientations. C: The decomposition of the calculated scattering intensities given off by the entire lipid phase (green line) into intensities given off by the two domains: the bilayer (blue line) and the micelle (red line). The sum of the intensities coming independently from the two domains is shown by the yellow line, which agrees well with the intensities produced by the two domains as a whole (green line).

micellar region). Of note, for SANS analyses, the scattering amplitudes, but not intensities, are additive and can be decomposed into components coming from various domains (50) (see Materials and Methods). Using this approach, we sought to determine the potential relative contribution of a bilayer versus micellar lipid packing organization to the scattering signal at different angles. Interestingly, the theoretical scattering intensities for neither the pure bilayer (blue line) nor the pure micellar (red line) lipid phases matched the experimental data (black open symbols). However, when computationally merged (yellow line), the composite of the two predicted domains demonstrated overall agreement with both the experimentally determined SANS scattering data (open symbols) and the theoretical SANS curve produced from the predicted lipid core of the Turtle model (green line, Fig. 9C).

This purely computational exercise thus seems to provide some further insights into the SANS analyses, since the theoretical scattering intensities generated at very small angles ($q < 0.1$ Å$^{-1}$) appear to predominantly arise from lipids within the bilayer domain, whereas at higher scattering angles ($q > 0.1$ Å$^{-1}$) the scattering intensities are predicted to come more so from the micellar domain (Fig. 9C). The overall goodness of fit observed for the SANS decomposition analysis strongly suggests that lipids within nHDL$_{DMPC}$ are packed as a mixture of lamellar and micellar phases. It is also important to realize this finding serves as an independent validation of the low-resolution structure of the protein observed (i.e., that it has an open conformation as a critical component).

### Expansion of the lipid cargo in nHDL is accommodated by loss of the apoA1 hairpin

We hypothesized that in an nHDL particle with a sufficiently large lipid cargo, the lipid can exert sufficient lateral pressure on the apoA1 domains that fold back into the hairpin to have the hairpin "unzip". Consequently, we prepared and analyzed by SANS nHDL$_{DMPC}$ particles that contain cholesterol nHDL$_{DMPC+Chol}$. Particle biochemical characterization confirmed a relatively homogeneous preparation with particles containing an apoA1 dimer, and an approximate 20% increase in lipid cargo (Fig. 1). The scattering intensities, the Guinier range, and the distance distribution function P(R) from SANS analyses of nHDL$_{DMPC+Chol}$ (prepared with deuterated apoA1) at 12% contrast (to directly visualize the protein component of the particle) are shown in **Fig. 10**. As before, multiple low-resolution shape envelopes for the protein were generated (supplementary Fig. IX) and the overall low resolution structure of apoA1 in nHDL$_{DMPC+Chol}$ obtained is depicted in various orientations in Fig. 10D. The protein structure observed is more clearly round (114 × 113 × 56 Å) and discoidal than that for nHDL$_{DMPC}$, but importantly, is still both open and with ends of the apoA1 dimer that are slightly out of plane. SANS analyses of nHDL$_{DMPC+Chol}$ at 42% contrast to directly visualize the lipid phase of the particle are shown in **Fig. 11** and supplementary Fig. X. The low-resolution structure of the lipid phase (Fig. 11) is overall ellipsoidal, though it seems more asymmetric than nHDL$_{DMPC}$.. Overall the protein and lipid shapes fit remarkably well with each other, like a lock and key, with a clearly discoidal overall particle (Fig. 11E).

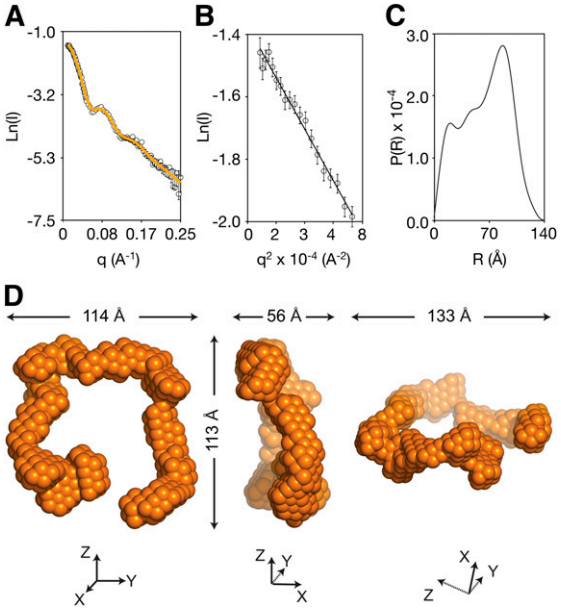


**Fig. 10.** nHDL$_{DMPC+Chol}$ in 12% $D_2O$. A: Logarithm of the scattering intensity versus the scattering vector, *q*. B: The Guinier plot was used to determine the radius of gyration. C: The distance distribution function P(R) was obtained by the deconvolution of the scattering intensities. D: The low resolution structure of the protein, component of nHDL$_{DMPC+Chol}$, in various orientations.

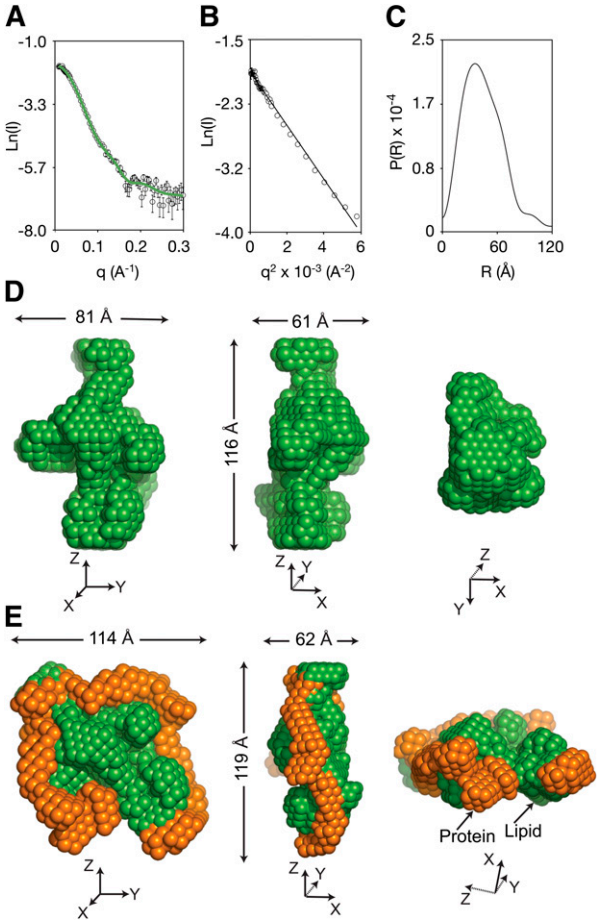


**Fig. 11.** nHDL$_{DMPC+Chol}$ in 42% $D_2O$. A: Logarithm of the scattering intensity versus the scattering vector, *q*. B: The Guinier plot. C: The P(R) function of the lipid component is smooth without additional decorations. as the function for the protein component, but decays more slowly at larger distances (>80 Å) when compared to the corresponding function for nHDL$_{DMPC}$. D: The low resolution structure of the lipid component of nHDL$_{DMPC}$ is shown in various orientations; the shape is not discoidal, rather asymmetric which may represent a bilayer with unequal leaflets capped by a small micellar domain. E: Overlap of the low-resolution structures. The protein component (12% $D_2O$, orange) is superimposed on the lipid component (green, 42% $D_2O$) of nHDL$_{DMPC}$. The two low-resolution structures fit as a key-in-a-lock.

### The protein structures observed by SANS analyses suggest a molecular mechanism accounting for the quantized sizes observed in nHDL particles

It is well recognized that the size of HDL particles is predominantly determined by the number of apoA1 incorporated per particle and its lipid cargo. Reconstituted HDL particles formed with apoA1 and varying amounts of DMPC (or other phospholipids) produce discrete well-defined sized particles predominantly containing two apoA1 chains [coined as R2 type (33)]. The molecular basis for the observed "quantized" size heterogeneity is ill defined, but has been suggested to arise from incremental incorporation of 11mer α-helical N-terminal domains into the closed apoA1 belt, a model referred to by Segrest and colleagues as the "hinge-domain" hypothesis (33, 54). A cartoon of this model is shown in **Fig. 12B** (upper row), and is readily visualized by a belt that can be enlarged by 11mer increments (colored in green) as it expands from one to another "belt hole". Indeed, in addition to nondenaturing gradient gel electrophoresis (33), a variety of biochemical studies are consistent with this model, including limited proteolysis (56, 57), antibody binding (58), and various spectroscopic techniques (57–60). However, as also noted by Segrest and colleagues (33), the molecular basis for the quantized expansion in nHDL size following the interaction of apoA1 and phospholipids is unknown.

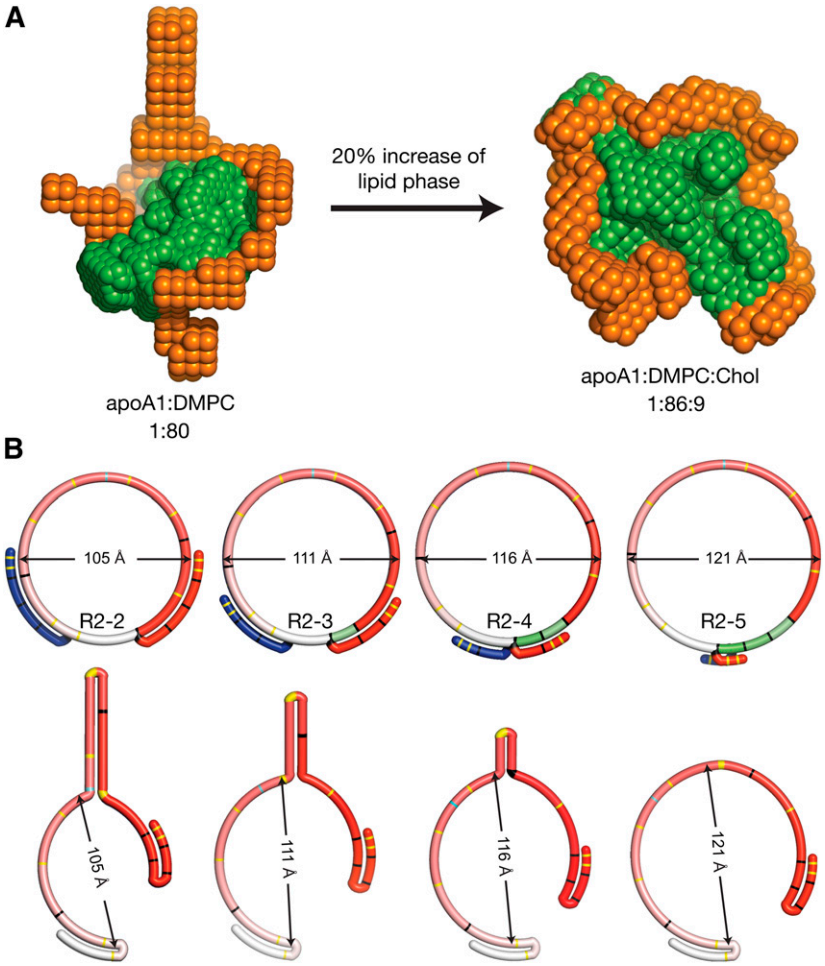


**Fig. 12.** Model for quantized nHDL particle expansion through unzipping of the apoA1 hairpin due to increase in lipid core. A: SANS shapes of $nHDL_{DMPC}$ and $nHDL_{DMPC+Chol}$ suggest unzipping of protein hairpin due to increase in lipid cargo. B: Top row: Mechanism for nHDL quantized expansion proposed by Li et al. (33). The apoA1 chain on top is colored red and the chain at the bottom is colored blue. The particle enlargement proceeds by the extension of apoA1 chains with one N-terminus 11mer (green) at a time, in order to accommodate the increase of the lipid phase. The locations of proline residues are marked with yellow, and the location of other residues that initiate an 11mer, are marked with black. The particles have been coined R2-2–R2-5 in the order of their increasing size. The original models do not show the full length of the N terminus, so in this figure the N termini are folded back. The residue 130, where helix 5 from the two chains is aligned, is marked with light blue. Bottom row: A cartoon representation of the Turtle model and the potential mechanism for quantized size expansion with increasing lipid cargo. nHDL particles of gradually increasing size are obtained by incrementally unfolding the hairpin with four 11mer units (from both chains) at a time. The four α-helical 11mers that form the hairpin are initially in mutual interaction along their hydrophobic surfaces, which is broken by the lateral pressure exerted by the lipids in the growing particle.





JOURNAL OF LIPID RESEARCH ASBMB

As illustrated by analyses of $nHDL_{DMPC}$ versus $nHDL_{DMPC+Chol}$ particle preparations herein, the present studies show that contrast variation SANS is quite sensitive to alterations in protein conformation induced by differences in lipid cargo content within the nHDL particle. Direct visualization of the structure within the protein component of nHDL provides an alternative molecular mechanism for the quantized size heterogeneity observed in nHDL. First, a key observation is that the global shape of the apoA1 dimer within nHDL is open, and not closed. Another key observation is that a large hairpin domain is clearly visible for the first time using contrast variation SANS in the $nHDL_{DMPC}$ particle with smaller lipid cargo. This direct experimental data reveals the hinge domain hypothesis, which depends upon the presence of a closed belt, is inaccurate. Rather, as a growing nHDL particle matures and expanding lipid content exerts lateral pressure on the apoA1 chains, there will be an incremental "unzipping" of the hairpin where the free energy of interaction between the hydrophobic protein interfaces on the hairpin is counterbalanced by the lateral pressure exerted by the expanding lipid core. This seems to happen each time when four 11mer increments (from both apoA1 chains), locked in mutual interaction, unzip and get exposed to lipids. One example is when cholesterol is added to the phospholipid (Fig. 12A) in reconstituted nHDL. In the present case the addition of cholesterol increased the lipid cargo by 20%, and this led to the unzipping of the hairpin. A cartoon of this hypothesis is illustrated in Fig. 12B (lower row). This quantized expansion seems to be facilitated by an α-helix breaking proline (yellow stripes in Fig. 12B) or other residue that caps an 11mer (black stripes), serving as a discrete "hinge".

Previous studies have suggested the presence of a hairpin within apoA1 of nHDL based upon alternative approaches. For example, Davidson and colleagues used a series of elegant site-specific mutants in which single tryptophan reporters and nitroxide spin quenchers were engineered within each of the 22 amino acid amphipathic helical repeats of apoA1. Differences observed with these apoA1 forms in tryptophan fluorescence between large (96 Å) and small (78 Å) nHDL particles produced, suggested a movable hinge domain exists within regions historically referred to as helices 5, 6, and/or 7, presumably allowing apoA1 to accommodate more or less lipid content (13). Resonance energy transfer studies using apoA1 mutants have also suggested the existence of an extended loop structure in the vicinity of residues 134–145 (helices 5 and 6) (12). In contrast to these prior approaches, which invariably require mutation of apoA1 and/or derivatization reactions, which can alter apoA1 conformation, the present studies provide a direct visualization of the apoA1 shape at low resolution, and are nonperturbing inasmuch as they require no mutations or derivatization.

### Structural similarities in nHDL models derived from SANS low-resolution structures point to common features among apolipoproteins

The two models of nHDL (DSH (15) and Turtle) and one model of spherical HDL [helical dimer hairpin loop (26)] have thus far been constructed from contrast variation SANS data (supplementary Fig. XI). Comparisons among these reveal similarities, suggesting that there are structural features shared by many apolipoproteins. First, apoA1 within both nHDL models and the spherical HDL model have an open conformation with sets off N/C-termini of apoA1 apart. This is in contrast to the discoidal model (and other twisted/bended simulation models), in which an apoA1 dimer forms a closed loop with the N/C-termini coming together (in truncated Δ43 apoA1). Second, in all contrast variation SANS-based models, the protein conformation is contorted and out of plane, a feature that is likely imparted by the presence of repeating proline residues which accentuate the bends in conformation. Of note, some discoidal models obtained by simulation bend out of plane, but they always remain closed loops (16–18). Another structural feature that sets apart the contrast variation SANS (direct experimental observation) versus simulation (hypothetical) models is the conformation of the N/C-termini. In all HDL structural models based upon direct visualization of protein shapes using contrast variation SANS thus far (14, 15, 27), the N/C-termini are predicted to fold back (**Fig. 13A**). Bhat et al. (11) first suggested the existence of this feature of apoA1 based on mass spectrometry cross-linking experiments. It is likely the two sets of termini in nHDL "stay apart". This forces "end-capping" phospholipids in micellar configuration to connect the two leaves of the bilayer within the central lipid domain of nHDL. It may be that this behavior (N/C-termini folding back and staying apart) is imprinted within the primary sequence of apoA1, and it is tempting to speculate that the endcap containing micellar lipid configuration in HDL may even impart unique biological activity. For example, it is well-known that many lipases, and other proteins that act at a lipid interface, can function even more efficiently on a micellar surface (61, 62).

Another remarkable similarity among SANS based models is that, regardless of lipid composition, they have the same radius of gyration ($R_g$ = ~52Å), and very similar overall dimensions (Table 1 and Table 1A of Ref. 15). The Belt model has $R_g$ = ~49 Å, and the $R_g$ for the bended simulation models is even lower (Table 1). Finally, in the contrast variation SANS-based models, the very nature of the open protein conformation allows individual lipids to diffuse freely throughout the entire lipid phase. This aspect may be essential for the ability of the particle to function as a cholesterol carrier because the lipid phase does not raise a free energy barrier to cholesterol diffusion through the entire lipid phase, and thus any cholesterol molecule within the lipid phase can access LCAT when bound to nHDL with the same easiness (i.e., there is no sidedness, like "heads" or "tails" of a coin, to the bilayer lipids as they can diffuse freely across the micellar end cap domain).

### Geometrical analysis of the apoA1 three-dimensional model for $nHDL_{DMPC}$ shows that major bends in protein conformation correspond mostly to proline positions

As mentioned above, the locations of proline residues in apoA1 of nHDL are believed to be associated with hinge

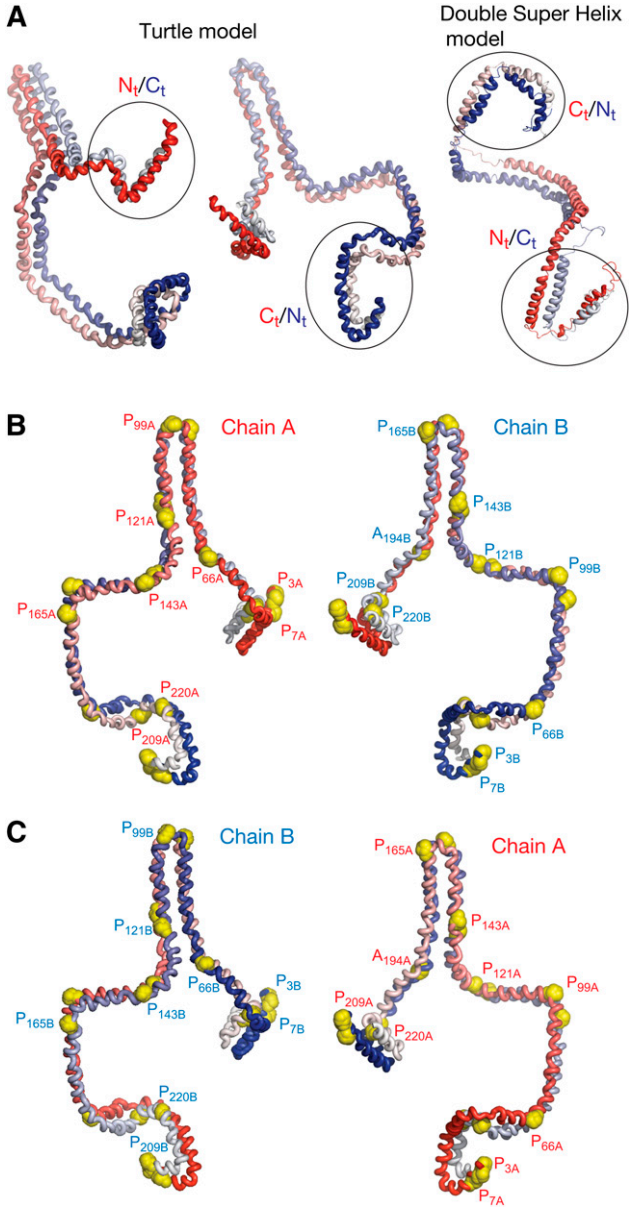


**Fig. 13.** Conformations of the N/C-termini in the Turtle and Double Super Helix models of nHDL. A: Left structure shows the N terminus of chain A (solid red) and the C terminus of chain B (light blue) of apoA1 in the Turtle model. The center structure shows the N terminus of chain B (solid blue) and the C terminus of chain A (light red). The right structure shows the N/C termini in the Double Super Helix model. Both models have in common the fact that the N/C-termini fold back (encircled regions) and are not joined together as in the Belt model. B: The overall conformation of the apoA1 dimer in the Turtle model of $nHDL_{DMPC}$. This pair of structures (front and back views) illustrates the overall conformation of apoA1 in which the hairpin is located within the N terminus of chain A (red) and C terminus of chain B. C: This pair of structures (front and back views) illustrates the overall conformation of apoA1 in which the hairpin is located within the C terminus of chain A (red) and N terminus of chain B. B and C: Proline residues are shown as yellow spheres, the N terminus is dark red or blue and the C terminus is light red or blue. The location of $A_{194}$ in each structure is also indicated. Residues at the base of the hairpin that serve as predicted hinges for all structures depicted include: $P_{66}$, $P_{121}$, $P_{143}$, and $A_{194}$. Note that $A_{194}$ in each structure is directly adjacent to $P_{66}$ from the antiparallel chain.

domains through which lipid-free apoA1 incrementally unfolds to accommodate particle enlargement (33). Interestingly, inspection of the Turtle model of $nHDL_{DMPC}$ reveals that most prolines are located at positions where major bends in apoA1 occur (Fig. 13B). For example, $P_{99A}$ and $P_{165B}$ (which are in close proximity) are located at the summit of the hairpin folds. Another pair of prolines, $P_{66A}$ and $P_{121B}$, is close to the starting points of the hairpin. Another striking aspect of the conformation of apoA1 in the Turtle model is that the "Solar Flare" regions of the apoA1 chains (14), putative sites of LCAT interaction ($L_{159}$-$A_{180}$), are not equivalent. Virtually all "belt type" models have a significant degree of symmetry. In contrast, within the Turtle model, the solar flare positioned within the hairpin is not accessible to the lipid, which might suppress the LCAT activity at this location.

Also illustrated in Fig. 13B, C is the concept that while the individual $HDL_{DMPC}$ structure itself lacks symmetry, the $nHDL_{DMPC}$ will be comprised of a pair of indistinguishable symmetrically related structures. This is because the particles are generated from an antiparallel pair of identical apoA1 chains. To illustrate this point, the pair of structures shown in Fig. 13B are two views (front and back) of an $nHDL_{DMPC}$ formed with the hairpin located in the N terminus of chain A (between $P_{66}$ and $P_{143}$) and the C terminus of chain B (between $P_{121}$ and $A_{194}$). Note that while there is no proline between $P_{165B}$ and $P_{209B}$, a residue with a relatively small and nonbulky side chain, $A_{194B,}$ is directly adjacent (opposite) to $P_{66A}$ of chain A, and readily accommodates the predicted bend in chain B opposite to $P_{66}$ of chain A at the base of the hairpin. The structures in Fig. 13C are the same two views of an alternative $nHDL_{DMPC}$ where the hairpin is instead located in the C terminus of the A chain (between $P_{121}$ and $A_{194}$) and the N terminus of chain B (between $P_{66}$ and $P_{143}$). Note that in $HDL_{DMPC}$ structures depicted (Fig. 13B, C) the A chain is colored red and the B chain is colored blue (N terminus dark and C terminus light for each). Thus, there is a 50% chance that the hairpin is located in either the N or C terminus of apoA1, and the two forms of $nHDL_{DMPC}$ cannot be distinguished (in both structures the hairpin is between $P_{66}$ and $P_{143}$ of one chain and $P_{121}$ and $A_{194}$ of the other chain). While the $nHDL_{DMPC}$ structures shown in Fig. 13B and 13C themselves do not contain a $C_2$ axis of symmetry [like the crystal structures of lipid-free N terminal or C terminal truncated mutant forms of apoA1 (19, 20)], it is evident that the $nHDL_{DMPC}$ are related by a form of symmetry.

Lipoproteins are involved in many biological functions, one of which is sterol and lipid transport. Despite their essential role in many physiological processes, efforts thus far to solve their crystal structure in the presence of lipid has been unsuccessful, most likely due to their heterogeneous composition and dynamic nature when lipidated. The application of SANS with contrast variation to the structural interrogation of $nHDL_{DMPC}$ enabled us to directly visualize a time-averaged low-resolution structure for the protein and lipid components of nHDL individually, and has revealed an unexpected conformation of





JOURNAL OF LIPID RESEARCH ASBMB

apoA1, a contorted open structure with a prominent hairpin that restricts the access of the lipid to only a portion of the hydrophobic surface of the protein. But, like the case of $nHDL_{POPC}$, the protein in $nHDL_{DMPC}$ offers mechanical strength to the HDL particle, while mediating lipid binding/transport and specific interactions with other proteins, like plasma enzymes and cell receptors. The observed open shape of apoA1 and the mixed packing (predominantly bilayer) of the lipid accounts for the experimental SANS intensities, while alternative shapes of the protein obtained by computer simulation do not (e.g., supplementary Figs. XI, XII).

In conclusion, we used contrast variation SANS to interrogate the structure of a reconstituted nHDL particle comprised of DMPC:apoA1 (80:1), a classic composition studied in numerous other investigations (9, 16, 22, 33, 53), as well as a particle with expanded lipid cargo. The results reveal overall shapes of both particles that are consistent with prior discoidal models of nHDL, in the sense that most of the lipid phase is predicted from SANS analysis to be lamellar packed, and the overall dimensions are of oblate ellipsoids. However, the protein shapes directly visualized within either $nHDL_{DMPC}$ or $nHDL_{DMPC+Chol}$ are clearly not classic belt configurations commonly envisaged; rather, the protein architecture of apoA1 within $nHDL_{DMPC}$ and $nHDL_{DMPC+Chol}$ both have an open configuration. The direct visualization for the first time of a presumptive hairpin loop by SANS within $nHDL_{DMPC}$, combined with both the confirmatory cross-linking mass spectrometry studies and the absence of a hairpin within the expanded lipid cargo particle, $nHDL_{DMPC+Chol}$, posit a molecular and structural mechanism for the well-known quantized size increases of nHDL during particle maturation. Moreover, the distinct environments experienced by the same sequences on distinct antiparallel apoA1 chains within nHDL explains the origin of bimodal exchange patterns observed during HDX studies.

## REFERENCES


1. Tall, A. R., L. Yvan-Charvet, N. Terasaka, T. Pagler, and N. Wang. 2008. HDL, ABC transporters, and cholesterol efflux: implications for the treatment of atherosclerosis. *Cell Metab.* **7:** 365–375.
2. Trigatti, B., A. Rigotti, and M. Krieger. 2000. The role of the high-density lipoprotein receptor SR-BI in cholesterol metabolism. *Curr. Opin. Lipidol.* **11:** 123–131.
3. Barter, P. J., and K. A. Rye. 2006. Relationship between the concentration and antiatherogenic activity of high-density lipoproteins. *Curr. Opin. Lipidol.* **17:** 399–403.
4. Rader, D. J. 2007. Mechanisms of disease: HDL metabolism as a target for novel therapies. *Nat. Clin. Pract. Cardiovasc. Med.* **4:** 102–109.
5. Assmann, G., and A. M. Gotto, Jr. 2004. HDL cholesterol and protective factors in atherosclerosis. *Circulation.* **109:** III8–III14.
6. Davidson, W. S., and T. B. Thompson. 2007. The structure of apolipoprotein A-I in high density lipoproteins. *J. Biol. Chem.* **282:** 22249–22253.
7. Thomas, M. J., S. Bhat, and M. G. Sorci-Thomas. 2008. Three-dimensional models of HDL apoA-I: implications for its assembly and function. *J. Lipid Res.* **49:** 1875–1883.
8. Phillips, J. C., W. Wriggers, Z. Li, A. Jonas, and K. Schulten. 1997. Predicting the structure of apolipoprotein A-I in reconstituted high-density lipoprotein disks. *Biophys. J.* **73:** 2337–2346.
9. Segrest, J. P., M. K. Jones, A. E. Klon, C. J. Sheldahl, M. Hellinger, H. De Loof, and S. C. Harvey. 1999. A detailed molecular belt model for apolipoprotein A-I in discoidal high density lipoprotein. *J. Biol. Chem.* **274:** 31755–31758.
10. Koppaka, V., L. Silvestro, J. A. Engler, C. G. Brouillette, and P. H. Axelsen. 1999. The structure of human lipoprotein A-I. Evidence for the "belt" model. *J. Biol. Chem.* **274:** 14541–14544.
11. Bhat, S., M. G. Sorci-Thomas, E. T. Alexander, M. P. Samuel, and M. J. Thomas. 2005. Intermolecular contact between globular N-terminal fold and C-terminal domain of apoA-I stabilizes its lipid-bound conformation: studies employing chemical cross-linking and mass spectrometry. *J. Biol. Chem.* **280:** 33015–33025.
12. Martin, D. D., M. S. Budamagunta, R. O. Ryan, J. C. Voss, and M. N. Oda. 2006. Apolipoprotein A-I assumes a "looped belt" conformation on reconstituted high density lipoprotein. *J. Biol. Chem.* **281:** 20418–20426.
13. Maiorano, J. N., R. J. Jandacek, E. M. Horace, and W. S. Davidson. 2004. Identification and structural ramifications of a hinge domain in apolipoprotein A-I discoidal high-density lipoproteins of different size. *Biochemistry.* **43:** 11717–11726.
14. Wu, Z., M. A. Wagner, L. Zheng, J. S. Parks, J. M. Shy III, J. D. Smith, V. Gogonea, and S. L. Hazen. 2007. The refined structure of nascent HDL reveals a key functional domain for particle maturation and dysfunction. *Nat. Struct. Mol. Biol.* **14:** 861–868.
15. Wu, Z., V. Gogonea, X. Lee, M. A. Wagner, X-M. Li, Y. Huang, U. Arundhati, R. P. May, M. Haertlein, M. Moulin, et al. 2009. Double superhelix model of high density lipoprotein. *J. Biol. Chem.* **284:** 36605–36619.
16. Gu, F., M. K. Jones, J. Chen, J. C. Patterson, A. Catte, W. G. Jerome, L. Li, and J. P. Segrest. 2010. Structures of discoidal high density lipoproteins: a combined computational-experimental approach. *J. Biol. Chem.* **285:** 4652–4665.
17. Li, L., S. Li, M. K. Jones, and J. P. Segrest. 2012. Rotational and hinge dynamics of discoidal high density lipoproteins probed by interchain disulfide bond formation. *Biochim. Biophys. Acta.* **1821:** 481–489.
18. Jones, M. K., L. Zhang, A. Catte, L. Li, M. N. Oda, G. Ren, and J. P. Segrest. 2010. Assessment of the validity of the double superhelix model for reconstituted high density lipoproteins: a combined computational-experimental approach. *J. Biol. Chem.* **285:** 41161–41171.
19. Borhani, D. W., D. P. Rogers, J. A. Engler, and C. G. Brouillette. 1997. Crystal structure of truncated human apolipoprotein A-I suggests a lipid-bound conformation. *Proc. Natl. Acad. Sci. USA.* **94:** 12291–12296.
20. Mei, X., and D. Atkinson. 2011. Crystal structure of C-terminal truncated apolipoprotein A-I reveals the assembly of high density lipoprotein (HDL) by dimerization. *J. Biol. Chem.* **286:** 38570–38582.
21. Bhat, S., M. G. Sorci-Thomas, R. Tuladhar, M. P. Samuel, and M. J. Thomas. 2007. Conformational adaptation of apolipoprotein A-I to discretely sized phospholipid complexes. *Biochemistry.* **46:** 7811–7821.
22. Silva, R. A. G. D., G. M. Hillard, L. Li, J. P. Segrest, and W. S. Davidson. 2005. A mass spectrometric determination of the conformation of dimeric apolipoprotein A-I in discoidal high density lipoproteins. *Biochemistry.* **44:** 8600–8607.
23. Chetty, P. S., L. Mayne, S. Lund-Katz, D. Stranz, S. W. Englander, and M. C. Phillips. 2009. Helical structure and stability in human apolipoprotein A-I by hydrogen exchange and mass spectrometry. *Proc. Natl. Acad. Sci. USA.* **106:** 19005–19010.
24. Sevugan Chetty, P., L. Mayne, Z-Y. Kan, S. Lund-Katz, S. W. Englander, and M. C. Phillips. 2012. Apolipoprotein A-I helical structure and stability in discoidal high-density lipoprotein (HDL) particles by hydrogen exchange and mass spectrometry. *Proc. Natl. Acad. Sci. USA.* **109:** 11687–11692.
25. Zhang, L., and G. Ren. 2012. IPET and FETR: experimental approach for studying molecular structure dynamics by cryo-electron tomography of a single-molecule structure. *PLoS ONE.* **7:** e30249.
26. Wu, Z., V. Gogonea, X. Lee, M. J. May, V. Pipich, M. A. Wagner, A. Undurti, T. C. Tallant, C. Baleanu-Gogonea, F. Charlton, et al. 2011. The low resolution structure of ApoA1 in spherical high density lipoprotein revealed by small angle neutron scattering. *J. Biol. Chem.* **286:** 12495–12508.
27. Gogonea, V., Z. Wu, X. Lee, V. Pipich, X-M. Li, A. I. Ioffe, J. A. DiDonato, and S. L. Hazen. 2010. Congruency between biophysical data from multiple platforms and molecular dynamics simulation of the double-super helix model of nascent high-density lipoprotein. *Biochemistry.* **49:** 7323–7343.

28. Matz, C. E., and A. Jonas. 1982. *J. Biol. Chem.* **257:** 4535–4540.
29. Wlodawer, A., J. P. Segrest, B. H. Chung, R. Chiovetti, Jr., and J. N. Weinstein. 1979. High-density lipoprotein recombinants: evidence for bicycle tire micelle structure obtained by neutron scattering and electron spectroscopy. *FEBS Lett.* **104:** 231–235.
30. Ramakrishnan, V. 1986. Distribution of protein and RNA in the 30S ribosomal subunit. *Science.* **231:** 1562–1564.
31. May, R. P., V. Nowotny, P. Nowotny, H. Voss, and K. H. Nierhaus. 1992. Inter-protein distances within the large subunit from Escherichia coli ribosomes. *EMBO J.* **11:** 373–378.
32. Willumeit, R., G. Diedrich, S. Forthmann, J. Beckmann, R. P. May, H. B. Stuhrmann, and K. H. Nierhaus. 2001. Mapping proteins of the 50S subunit from Escherichia coli ribosomes. *Biochim. Biophys. Acta.* **1520:** 7–20.
33. Li, L., J. Chen, V. K. Mishra, J. A. Kurtz, D. Cao, A. E. Klon, S. C. Harvey, G. M. Anantharamaiah, and J. P. Segrest. 2004. Double belt structure of discoidal high density lipoproteins: molecular basis for size heterogeneity. *J. Mol. Biol.* **343:** 1293–1311.
34. Peng, D. Q., Z. Wu, G. Brubaker, L. Zheng, M. Settle, E. Gross, M. Kinter, S. L. Hazen, and J. D. Smith. 2005. Tyrosine modification is not required for myeloperoxidase-induced loss of apolipoprotein A-I functional activities. *J. Biol. Chem.* **280:** 33775–33784.
35. Baker, P. W., K. A. Rye, J. R. Gamble, M. A. Vadas, and P. J. Barter. 2000. Phospholipid composition of reconstituted high density lipoproteins influences their ability to inhibit endothelial cell adhesion molecule expression. *J. Lipid Res.* **41:** 1261–1267.
36. Guinier, A. 1939. La diffraction des rayons X aux tres petits angles; application a l'etude de phenomenes ultramicroscopiques. *Ann. Phys.* **12:** 161–237.
37. Svergun, D. I. 1992. Determination of the regularization parameter in indirect-transform methods using perceptual criteria. *J. Appl. Crystallogr.* **25:** 495–503.
38. Svergun, D. I. 1999. Restoring low resolution structure of biological macromolecules from solution scattering using simulated annealing. *Biophys. J.* **76:** 2879–2886.
39. Merzel, F., and J. C. Smith. 2002. SASSIM: a method for calculating small-angle X-ray and neutron scattering and the associated molecular envelope from explicit-atom models of solvated proteins. *Acta Crystallogr. D Biol. Crystallogr.* **58:** 242–249.
40. Panchaud, A., P. Singh, S. A. Shaffer, and D. R. Goodlett. 2010. xComb: a cross-linked peptide database approach to protein-protein interaction analysis. *J. Proteome Res.* **9:** 2508–2515.
41. Clauser, K. R., P. R. Baker, and A. L. Burlingame. 1999. Role of accurate mass measurement (+/− 10 ppm) in protein identification strategies employing MS or MS/MS and database searching. *Anal. Chem.* **71:** 2871–2882.
42. Svergun, D. I., C. Barberato, and M. H. J. Koch. 1995. CRYSOL—a program to evaluate X-ray solution scattering of biological macromolecules from atomic coordinates. *J. Appl. Crystallogr.* **28:** 768–773.
43. MacKerell, A. D., Jr., D. Bashford, M. Bellot, R. L. Dunbrack, Jr., J. Evanseck, M. J. Field, S. Fischer, J. Gao, H. Guo, S. Ha, et al. 1998. All-atom empirical potential for molecular modeling and dynamics studies of proteins. *J. Phys. Chem. B.* **102:** 3586–3616.
44. MacKerell, A. D., Jr., N. Banavali, and N. Foloppe. 2000–2001. Development and current status of the CHARMM force field for nucleic acids. *Biopolymers.* **56:** 257–265.
45. Jorgensen, W. L., J. Chandrasekhar, and J. D. Madura. 1983. Comparison of simple potential functions for simulating liquid water. *J. Chem. Phys.* **79:** 926–935.
46. Hess, B., C. Kutzner, D. Van Der Spoel, and E. Lindahl. 2008. GROMACS 4: algorithms for highly efficient, load-balanced, and scalable molecular simulation. *J. Chem. Theory Comput.* **4:** 435–447.
47. Darden, T., D. York, and L. Pedersen. 1993. Particle mesh Ewald: an N-log(N) method for Ewald sums in large systems. *J. Chem. Phys.* **98:** 10089–10092.
48. Essmann, U., L. Perera, M. L. Berkowitz, T. Darden, H. Lee, and L. G. Pedersen. 1995. A smooth particle mesh Ewald potential. *J. Chem. Phys.* **103:** 8577–8592.
49. Serdyuk, I. N., N. R. Zaccai, and J. Zaccai, editors. 2007. Methods in Molecular Biophysics. Cambridge University Press, Cambridge, UK.
50. Svergun, D. I., and M. H. J. Koch. 2003. Small-angle scattering studies of biological macromolecules in solution. *Rep. Prog. Phys.* **66:** 1735–1782.
51. Roosbeek, S., B. Vanloo, N. Duverger, H. Caster, J. Breyne, I. De Beun, H. Patel, J. Vandekerckhove, C. Shoulders, M. Rosseneu, et al. 2001. Three arginine residues in apolipoprotein A-I are critical for activation of lecithin:cholesterol acyltransferase. *J. Lipid Res.* **42:** 31–40.
52. Li, H-H., D. S. Lyles, W. Pan, E. Alexander, M. J. Thomas, and M. G. Sorci-Thomas. 2002. ApoA-I structure on discs and spheres. Variable helix registry and conformational states. *J. Biol. Chem.* **277:** 39093–39101.
53. Segrest, J. P. 1977. Amphipathic helixes and plasma lipoproteins: thermodynamic and geometric considerations. *Chem. Phys. Lipids.* **18:** 7–22.
54. Brouillette, C. G., J. L. Jones, T. C. Ng, H. Kercret, B. H. Chung, and J. P. Segrest. 1984. Structural studies of apolipoprotein A-I/phosphatidylcholine recombinants by high-field proton NMR, nondenaturing gradient gel electrophoresis, and electron microscopy. *Biochemistry.* **23:** 359–367.
55. Zhu, K., G. Brubaker, and J. D. Smith. 2007. Large disk intermediate precedes formation of apolipoprotein A-I-dimyristoylphosphatidylcholine small disks. *Biochemistry.* **46:** 6299–6307.
56. Calabresi, L., G. Tedeschi, C. Treu, S. Ronchi, D. Galbiati, S. Airoldi, C. R. Sirtori, Y. Marcel, and G. Franceschini. 2001. Limited proteolysis of a disulfide-linked apoA-I dimer in reconstituted HDL. *J. Lipid Res.* **42:** 935–942.
57. Roberts, L. M., M. J. Ray, T. W. Shih, E. Hayden, M. M. Reader, and C. G. Brouillette. 1997. Structural analysis of apolipoprotein A-I: limited proteolysis of methionine-reduced and -oxidized lipid-free and lipid-bound human apo A-I. *Biochemistry.* **36:** 7615–7624.
58. Bergeron, J., P. G. Frank, D. Scales, Q. H. Meng, G. Castro, and Y. L. Marcel. 1995. Apolipoprotein A-I conformation in reconstituted discoidal lipoproteins varying in phospholipid and cholesterol content. *J. Biol. Chem.* **270:** 27429–27438.
59. Calabresi, L., G. Vecchio, F. Frigerio, L. Vavassori, C. R. Sirtori, and G. Franceschini. 1997. Reconstituted high-density lipoproteins with a disulfide-linked apolipoprotein A-I dimer: evidence for restricted particle size heterogeneity. *Biochemistry.* **36:** 12428–12433.
60. Okon, M., P. G. Frank, Y. L. Marcel, and R. J. Cushley. 2002. Heteronuclear NMR studies of human serum apolipoprotein A-I. Part I. Secondary structure in lipid mimetic solution. *FEBS Lett.* **517:** 139–143.
61. Deems, R. A. 2000. Interfacial enzyme kinetics at the phospholipid/water interface: practical considerations. *Anal. Biochem.* **287:** 1–16.
62. Burke, J. E., and E. A. Dennis. 2009. Phospholipase A2 structure/function, mechanism, and signaling. *J. Lipid Res.* **50:** S237–S242.